Parameterized atmospheric reactivity and oxidation capacity during summer at a suburban site between Beijing and Tianjin

Yuan Yang[1,2], Yonghong Wang[3], Putian Zhou[3,4], Dan Yao[1,2,5], Dongsheng Ji[1], Jie Sun[1], Yinghong Wang[1], Shuman Zhao[1,2], Wei Huang[1,2], Shuanghong Yang[1,5], Dean Chen[3], Wenkang Gao[1], Zirui Liu[1], Bo Hu[1], Renjian Zhang[1], Limin Zeng[6], Maofa Ge[7], Tuukka Petäjä[3], Veli-Matti Kerminen[3], Markku Kulmala[3], Yuesi Wang[1,2,8]

[1] Institute of Atmospheric Physics, Chinese Academy of Sciences, Beijing 100029, China

[2] University of the Chinese Academy of Sciences, Beijing 100049, China

[3] Institute for Atmospheric and Earth System Research / Physics, Faculty of Science, P.O.Box 64, 00014 University of Helsinki, Helsinki, Finland

[4]Climate and Marine Sciences Department, Eurasia Institute of Earth Sciences, Istanbul Technical University, Maslak 34469, Istanbul, Turkey

[5]Department of Environmental Science and Engineering, Beijing University of Chemical Technology, Beijing 10029, China

[6]State Joint Key Laboratory of Environmental Simulation and Pollution Control, College of Environmental Sciences and Engineering, Peking University, Beijing 100871, China

[7] State Key Laboratory for Structural Chemistry of Unstable and Stable Species, CAS Research/Education Center for Excellence in Molecular Sciences, Institute of Chemistry, Chinese Academy of Sciences, Beijing 100190, China

[8] Center for Excellence in Regional Atmospheric Environment, Institute of Urban Environment, Chinese Academy of Sciences, Xiamen 361021, China

Revised to: Atmospheric Chemistry and Physics

Corresponding to: Yonghong Wang, yonghong.wang@helsinki.fi; Yuesi Wang, wys@mail.iap.ac.cn

Abstract

Hydroxyl (OH) radicals, nitrate (NO_3) radicals, and ozone (O_3) play central roles in the troposphere because they control the lifetimes of many trace gases that result from anthropogenic and biogenic origins. To estimate the air chemistry, the atmospheric reactivity and oxidation capacity was comprehensively analyzed based on a parameterization method at a suburban site in Xianghe in the North China Plain from 6 July 2018 to 6 August 2018. The total OH, NO_3 and O_3 reactivities at the site varied from 9.2 s^{-1} to 69.6 s^{-1}, 0.7 s^{-1} to 27.5 s^{-1} and 3.3×10^{-4} s^{-1} to 1.8×10^{-2} s^{-1} with campaign-averaged values of 27.5±9.7 s^{-1}, 2.2±2.6 s^{-1} and $1.2\pm1.7\times10^{-3}$ s^{-1} (± standard deviation), respectively. NO_x ($NO+NO_2$) were by far the main contributors to the three oxidants reactivities, with average values of 43-99%. Alkenes dominated the OH, NO_3 and O_3 reactivities towards total non-methane volatile organic compounds (NMVOCs), accounting for 42.9%, 77.8% and 94.0%, respectively. The total OH, NO_3 and O_3 reactivities displayed a similar diurnal variation with the lowest during the afternoon but the highest during the rush hours, and the diurnal profile of NO_x appears to be the major driver for the diurnal profiles of the three oxidant reactivities. A box model SOSAA (a model to Simulate the concentrations of Organic vapors, Sulfuric Acid and Aerosol) derived from a column chemical transport model was used to simulate OH and NO_3 concentrations during the observation period. The calculated atmospheric oxidation capacity (AOC) was up to 4.5×10^{8} molecules cm^{-3} s^{-1} with campaign-averaged values of 7.8×10^{7} molecules cm^{-3} s^{-1} dominated by OH (7.7×10^{7} molecule cm^{-3} s^{-1}, 98.2%), O_3 (1.2×10^{6} molecule cm^{-3} s^{-1}, 1.5%) and NO_3 (1.8×10^{5} molecule cm^{-3} s^{-1}, 0.3%). Overall, the present study may provide some useful suggestions for VOCs pollution control in the Xianghe and North China Plain. We suggest that further studies, especially direct observations of OH and NO_3 radicals concentrations and their reactivities, are required to better understanding the trace gas reactivity and AOC.

Keywords:

VOCs, atmospheric oxidants reactivity, atmospheric oxidation capacity, North China Plain

1 Introduction

In the planetary boundary layer, high concentrations of primary pollutants, such as carbon monoxide (CO), nitrogen oxides (NO_x=$NO+NO_2$) and volatile organic compounds (VOCs) from

both biogenic and anthropogenic origins, are transformed by reactions with atmospheric oxidants, such as hydroxyl (OH) radicals, nitrate (NO_3) radicals, chlorine atom and ozone (O_3) on local to global scales (Atkinson and Arey, 2003; Heard and Pilling, 2003; Lu et al., 2018), with the dominant reaction depending on the time of day and specific trace gases. Ultimately, these processes lead to the formation of a series of important secondary pollutants, including tropospheric O_3 and secondary organic aerosol (SOA) (Goldstein and Galbally, 2007).

OH radicals control the daytime oxidation capacity of the atmosphere (Heard and Pilling, 2003), initiating and participating in many oxidation reaction processes. OH exhibits a high reactivity to many atmospheric trace gases, such as CO, NO_x, methane (CH_4), non-methane volatile organic compounds (NMVOCs) (Kovacs et al., 2003; Sadanaga et al., 2005). The total OH reactivity is the sum of the products of the concentrations and respective reaction rate coefficients for all gases that react with OH. The total OH reactivity is equivalent to the inverse of the lifetime of OH (s^{-1}) in the presence of those atmospheric constituents that can be either measured directly, modeled or calculated from individual trace gas measurements. The online techniques used to determine OH reactivity include the flow tube with sliding injector method (Kovacs et al., 2003), a comparative rate method (Sinha et al., 2008) and a laser flash photolysis pump probe technique (Whalley et al., 2016). Based on these online methods, the values of total OH reactivity have been measured in urban, suburban, remote and forest areas during the last decade. The urban areas investigated included Nashville, USA (SOS) (Kovacs et al., 2003), New York, USA (PMTACS-NY2004) (Ren et al., 2006a), Mexico City, Mexico (MCMA-2003) (Shirley et al., 2006), Houston, USA (TRAMP2006) (Mao et al., 2010), Paris, France (MEGAPOLI) (Dolgorouky et al., 2012), London, UK (ClearfLo) (Whalley et al., 2016), Helsinki, Finland (Praplan et al., 2017), Seoul, South Korea (Kim et al., 2016) and Beijing, China (Yang et al., 2017). The ranges of total OH reactivity in these urban areas ranged from 1 s^{-1} in clean air to 200 s^{-1} in extremely polluted air in the atmospheric boundary layer, and NO_x, CO, formaldehyde (HCHO) and NMVOCs were the main contributors (Ferracci et al., 2018). The suburban areas investigated included Whiteface Mountain, USA (PMTACS-NY2002) (Ren et al., 2006b), Weybourne, UK (TORCH-2) (Lee et al., 2010), Yufa, China (CAREBeijing-2006) (Lu et al., 2010), Backgarden, China (PRIDE-PRD) (Lou et al., 2010), Jülich, Germany (HOx Comp) (Elshorbany et al., 2012), Ersa, Corsica (CARBOSOR-ChArMeX)

(Zannoni et al., 2017), Po Valley, Italy (Kaiser et al., 2015), Indo-Gangetic Plain, India (Kumar et al., 2018) and Heshan, China (Yang et al., 2017). The ranges of total OH reactivity in these suburban areas ranged from 4.6 to 64 s^{-1}. The total OH reactivity was also modeled using a zero-dimensional box model based on the Regional Atmospheric Chemical Mechanism to compare them with the measurements or calculations (Lou et al., 2010; Whalley et al., 2016; Ferracci et al., 2018; Yang et al., 2017). The calculated total OH reactivity is the sum of the OH reactivities that are attributed to measured trace gases, which is used extensively as a metric to estimate the initial peroxyl radical (RO_2) formation rate under optimum reaction conditions (Carter, 2012; Liu et al., 2008; Warneke, 2004). This metric does not account for chain termination or propagation steps, nor does it properly capture differences in NMVOCs production of RO_2 during photolysis or reaction with other oxidants; however, this metric does provide at least some useful approximation of the relative contribution of individual NMVOCs to daytime photochemistry (Goldan et al., 2004; Benedict et al., 2019). The concentrations (in molecules cm^{-3}) of trace gases and the reaction rate constants (in cm^3 $molecule^{-1}$ s^{-1}) of the respective trace gases with the OH radical are the key factors for computing OH reactivity (Mogensen et al., 2011; Mogensen et al., 2015). In general, the trace gases considered in calculating OH reactivity include NMVOCs, CH_4, CO, NO_x, SO_2 and O_3. As reported, the contribution from NO_x exceeds 50% for the cities of Paris, Tokyo, New York and Beijing, showing the large influence of traffic-related emissions on the OH reactivity (Dolgorouky et al., 2012; Ren, 2003; Yang et al., 2017; Yoshino et al., 2006), but the contribution from the NMVOCs reaches 50% in Mexico and Houston due to high biomass fuel being burned and industrial solvent emissions (Mao et al., 2010; Shirley et al., 2006).

As OH levels are vastly reduced during nighttime due to missing photolysis, the NO_3 formed by the slow reaction of $NO_2 + O_3 \rightarrow NO_3 + O_2$ is the main initiator of nighttime oxidation chemistry in the troposphere at night (Asaf et al., 2009; Geyer et al., 2001). NO_3 reacts effectively with unsaturated NMVOCs, such as certain alkenes or aromatics, via additions to a >C=C< double bond, which can initiate the formation of peroxyl radicals (HO_2 and RO_2) and even of OH (Geyer et al., 2001). The high NO_3 mixing ratios and the large reaction rate constants with several unsaturated NMVOCs result in NO_3 being the dominant sink of many unsaturated NMVOCs during nighttime. The role of NO_3 as an oxidizing agent may be assessed via its total reactivity towards trace gases.

The total NO_3 reactivity is an indication of nighttime oxidation rates of trace gases with direct impacts on NO_x levels and indirect impacts on heterogeneous NO_x losses and $ClNO_2$ formation (Liebmann et al., 2017). As frequently reported for total OH reactivity, total NO_3 reactivity can be measured online or calculated from summing loss rates for a set of reactive trace gases. Previous work on total NO_3 reactivity measured has revealed a strong diel variation. For instance, the total NO_3 reactivity obtained in Hyytiälä, Finland (Influence of Biosphere-Atmosphere Interactions on the Reactive Nitrogen budget (IBAIRN) campaign), displayed a strong diel variation with a campaign-averaged nighttime mean value of 0.11 s^{-1} compared to a daytime value of 0.04 s^{-1} (Liebmann et al., 2018a), but varied from 0.005 to 0.1 s^{-1} during nighttime and reached values as high as 1.4 s^{-1} in the daytime at the Taunus, Germany (NOcturnal chemistry at the Taunus Observatorium: insights into Mechanisms of Oxidation (NOTOMO) campaign) (Liebmann et al., 2017).

Along with reactions with the OH and NO_3 radicals, trace gases are oxidized in the troposphere by reactions with O_3. Although for most NMVOCs, their reaction reaction rate with O_3 is much lower than that with either OH or NO_3, O_3 is very important because it is present at elevated mixing ratios in clean or contaminated atmospheres (Wang et al., 2013). The rate constants of the reactions for some alkenes with O_3 are even comparable to those with NO_3 (Atkinson and Arey, 2003). The total reaction of O_3 with trace gases can reflect the role of O_3 as an oxidizing agent. Direct measurements of total O_3 reactivity were not available until very recently (Geyer, 2003); hence, the reactivity of O_3 has traditionally been calculated by summing the reactivities due to individual reactive trace gases. The calculated O_3 reactivity obtained at Pabstthum, Germany (Berliner Ozonexperiment (BERLIOZ) campaign) revealed that terpenes (20%), isoprene (20%) and other alkenes (60%) were the dominant contributors during the night of 20 and 21 July but arose mainly (83%) from non-biogenic alkene during the night of 4 and 5 August (Geyer, 2003).

Recently, several studies on measured, modeled or calculated total OH reactivity have been conducted in China (Lou et al., 2010; Fuchs et al., 2017; Yang et al., 2017; Lu et al., 2010; Williams et al., 2016; Lyu et al., 2019). However, comprehensive evaluations of the total OH, NO_3 and O_3 reactivities calculated are scarce. In this study, we calculated the OH, O_3 and NO_3 reactivities at a suburban site (Xianghe) in the North China Plain during an intensive measurement campaign in the

summer of 2018. By combining simulated OH and NO_3 concentrations using a box model SOSAA, we calculated the oxidation capacities of OH, NO_3 and O_3 and estimated their relative contributions.

2 Methodology

2.1 Site description

The sampling site is located at the Xianghe Atmospheric Observatory (39.798 °N, 116.958 °E; 15 m above sea level), which is operated by the Institute of Atmospheric Physics (IAP)/Chinese Academy of Sciences (CAS). The sampling site is a typical suburban site in the seriously polluted Beijing-Tianjin-Hebei large urban region, which is approximately 50 km southeast of Beijing, 75 km northwest of Tianjin, and 35 km northeast of Langfang in the Hebei Province. The sampling site is approximately 4 km west of the downtown center and is surrounded by residential areas and agricultural land (see Figure 1).

2.2 Experimental method

O_3 was measured using a UV photometric O_3 analyzer (Model 49C/I, Thermo-Fisher Scientific, United States) with the detection limit of 2.0 ppb, precision of ±1.0 ppb, zero drift of less than 1.0 ppb $(24\ h)^{-1}$, span drift of less than 1% full scale per month, and response time of 10 s. NO_x was measured using a chemiluminescence NO_x Analyzer (Model 42C/I) with the detection limit of 0.4 ppb, precision of ±0.4 ppb, zero drift of less than 0.4 ppb $(24\ h)^{-1}$, span drift of less than 1% per 24 h, and response time of 40 s. NO_y was measured using a chemiluminescence NO-DIF-NOy Analyzer (Model 42C/I) with the detection limit of 50 ppt, span drift of less than 1% per 24 h, and response time of 60 s. SO_2 was measured using a pulsed fluorescence SO_2 analyzer (Model 43C/I) with the detection limit of 0.5 ppb, precision of 1% of reading or 1 ppb, zero drift of less than 1 ppb $(24\ h)^{-1}$, span drift of less than 0.5% full scale per 24 h, and response time of less than 20 s. CO was measured with a nondispersive infrared analyzer (Model 48I) with the detection limit of 0.4 ppm, a precision of 0.1 ppm, zero drift of less than 0.1 ppb $(24\ h)^{-1}$, span drift of less than 0.1% full scale per 24 h, and response time of less than 60 s. These measurement instruments were housed in a container that was equipped with an air conditioner. Ambient air samples were drawn through a 3-m PFA Teflon tube (outside diameter: 12.7 mm; inside diameter: 9.6 mm), and the sampling tube inlets were located 1m above the conditioner. High resolution (5 min averages) data sets of O_3, NO,

NOx, NOy, SO_2 and CO were obtained, and hourly averaged data were used after applying strict data quality control. The sampling methods and instrument protocols as well as quality assurance/quality control (QA/QC) procedures for air quality monitoring are described in detail in the Chinese National Environmental Protection Standard, Automated Methods for Ambient Air Quality Monitoring (HJ/T 193–2005; State Environmental Protection Administration of China, 2006). The measurement techniques are the same as those used in Wang et al. (2014) and Xin et al. (2012).

Ambient NMVOCs were collected and analyzed continuously and automatically with a time resolution of 1 h using a custom-built gas chromatography-mass spectrometry/flame ionization detector (GC-MS/FID). The online GC-MS/FID system consisted of three major components: a cryogen-free cooling device for creating ultra-low temperatures (TH300, Wuhan Tianhong Environmental protection industry co., LTD, Wuhan, China), a sampling and preconcentration system for NMVOCs collection and enrichment, and a gas chromatography (GC, 7820A, Agilent Technologies, Santa Clara, CA, USA) equipped with an MS and an FID (5977E, Agilent Technology, Santa Clara, CA, USA) for NMVOCs separation and detection. The custom-built online GC-MS/FID was a two-channel system and was capable of measuring C2-C12 hydrocarbons and selected C2-C5 carbonyls. The two channels have their own inlets, cold traps and GC separation columns, but they share one cryogenic source and programmed temperature procedure. The availability of this system for NMVOCs measurement are well verified and it has been used in several large field campaign (Chen et al., 2014; Yuan et al., 2013; Wu et al., 2016), and was described by our previous paper (Yang et al., 2019). Briefly, samples are collected into GC-MS/FID at a flow rate of 60 mL min^{-1} with sampling time of 5 min at the beginning of each hour. The sampling lines for ambient air and standard gases were both Teflon tubes with a 1/4-inch outside diameter (OD). A Teflon filter was placed in the inlet to prevent particulate matters from entering the instrument, and a water trap was used to remove H_2O from the air samples. Ascarite II was used to remove CO_2 and O_3 before the FID channel, whereas a Na_2SO_3 trap was used to remove O_3 in the MS channel. C2-C5 hydrocarbons were separated on a PLOT-Al_2O_3 column (15 m × 0.32 mm ID×3 μm, J&W Scientific, USA) and were measured by the FID channel. Other compounds were separated on a semi polar column (DB624, 60 m × 0.25 mm ID×1.4 μm, J&W Scientific, USA) and

were quantified using a quadrupole MS detector. The two columns were not exchanged during the intensive measurement campaign.

The compounds analyzed were subjected to rigorous quality assurance and quality control procedures (QA/QC). The NMVOCs detected by FID were quantified by the external standard method, and the components detected by MS were quantified by the internal standard method. Four compounds, i.e., bromochloromethane, 1,4-difluorobenzene, chlorobenzene-d5, and bromofluorobenzene, were used as internal standards. Specifically, the system was calibrated at multiple concentrations in the range of 0.8-8 ppb by two gas standards, i.e., a mixture of 57 PAMS (provided by Spectra Gases Inc., USA), and a mixture of oxygenated VOCs (OVOCs) and halocarbons (provided by Spectra Gases Inc., USA). R^2 values for the calibration curves ranged from 0.941 to 1.000 for NMVOCs, indicating that integral areas of the peaks were proportional to concentrations of target compounds. The method detection limit (MDL) of the online GC-FID/MS system for all measured compounds ranged from 0.003 to 0.092 ppb. The measurement relative standard deviation (RSD) for measured compounds ranged from 2.1% to 14.9% (Yang et al., 2019). To check the stability of the instrument, routine calibration was performed periodically by using a calibration gas with a mixing ratio of 2 ppb consisting of 56 kinds of NMVOCs components. The variations between the measured and nominal concentrations of the periodic calibration were within 10%. The signal variations of each targeted compound due to system instability were corrected by the signal of CFC-113 (1,1,2-trichloro-1,2,2-trifluoroethane) due to its long atmospheric lifetime and stable anthropogenic emissions (Yuan et al., 2013; Chen et al., 2014). Detailed instrumental and operational parameters are described in our previous study (Yang et al., 2019).

Measurements of atmospheric HONO mixing ratios were conducted using a custom-made HONO analyzer. The detailed information can be seen elsewhere (Zhang et al., 2019; Tong et al., 2015). CH_4 were analyzed by Agilent 7890A gas chromatography (GC) with flame ionization detector (FID). Standard samples were provided by NIST of USA and NSC of China. The precision of CH_4 concentration analysis is 0.05± 0.10%. HCHO was measured by Hantzsch Fluorimetry with a commercial instrument (AL4021, Aerolaser GmbH, Germany) (Lu et al., 2019).

The photolysis frequencies, JO^1D, JNO_2 and JNO_3, in the atmosphere are measured by the PFS-100 Photolysis Spectrometer (Juguang Technology (hangzhou) Co., Ltd, Hangzhou, China).

The photolysis rate is calculated by integrating the actinic flux with the known absorption cross section $\sigma(\lambda)$ and quantum yield $\varphi(\lambda)$. The actinic flux is spherically integrated photon radiance of the solar radiation in the atmosphere. The spectrometer obtains spectral information in a certain wavelength range, which mainly uses quartz receiver to collect solar radiation from all directions, and convert it into the actinic flux F_λ. $\sigma(\lambda)$ is the absorption cross section of the species that absorbs in certain wavelength range and $\varphi(\lambda)$ is quantum yield of the photodissociation reaction product; these two coefficients have been measured by experiments and can be directly looked up and used.

The meteorological parameters, including wind speed, wind direction, temperature and relative humidity were obtained from the National Meteorological Information Center (http://data.cma.cn/). The sensors are about 3000 meters away from the measurement area.

2.3 Atmospheric chemical transport model SOSAA

SOSAA (a model to Simulate the concentrations of Organic vapours, Sulfuric Acid and Aerosol) is a column (or one-dimensional) chemical transport model, which was first developed by Boy et al. (2011). A more detailed description of its newest version can be found in Zhou et al. (2017a) and Zhou et al. (2017b). In this study, a box model version of SOSAA was used, in which the meteorological variables, including air temperature, air pressure, relative humidity and incoming global radiation, were directly read from the measurement data. The chemistry scheme was generated by MCM v3.3.1 (Master Chemical Mechanism version 3.3.1, http://mcm.leeds.ac.uk/MCMv3.3.1) (Jenkin et al., 1997; Jenkin et al., 2015; Saunders et al., 2003) and then converted to Fortran code with KPP (kinetic pre-processor; Damian et al., 2002). The mixing ratios of chemical species included in the chemistry scheme were read from the measured data when available, e.g., O_3, NO, NO_2, SO_2, CO, HONO, HCHO, isoprene, acetone, etc. Ten OVOCs (ACR, C_2H_5CHO, MACR, C_3H_7CHO, MVK, MEK, MPRK, C_4H_9CHO, DIEK, $C_5H_{11}CHO$) were excluded from the input list although they were also measured, because their simulated concentrations were used to compare with the measurement data to validate the model performance. Seven photolysis rates (J_O^1D, J_HCHO_M, J_NO_2, $J\_H_2O_2$, J_HONO, J_NO_3_M, J_NO_3_R) were also read from the measurement data, the related photochemical reactions are shown below:

O_3 -> O_2 + O1D: J_O^1D (R1)

$HCHO \rightarrow H_2 + CO$: J_HCHO_M (R2)

$NO_2 \rightarrow NO + O^3P$: J_$NO_2$ (R3)

$H_2O_2 \rightarrow 2\ OH$: J_H_2O_2 (R4)

$HONO \rightarrow OH + NO$: J_HONO (R7)

$NO_3 \rightarrow NO + O_2$: J_$NO_3$_M (R8)

$NO_3 \rightarrow NO_2 + O^3P$: J_$NO_3$_R. (R9)

The other photolysis rates were calculated using the incoming global radiation. The deposition velocities of all non-input species were set to 0.01 m s^{-1} and the boundary layer height was assumed to be 1 km (Lu et al., 2013; Zhu et al., 2020). The simulated OVOCs were also considered to be condensing onto pre-existing aerosols. Their condensation sinks were set to make their simulated concentrations approach the measurement data. The model time step was set to 10 s, and the data were output every half an hour. All the input data were interpolated to the model time step.

2.4 Speciated oxidant reactivity

Atmospheric oxidant reactivity is a measure of the strength of reaction of trace gases to the oxidant (= OH, O_3, NO_3) (Kovacs et al., 2003; Mogensen et al., 2015). High oxidant reactivity values correspond to short lifetimes and long-lived species have low reactivities. The total OH, NO_3 and O_3 reactivities can be calculated by Eq. (1)-(3), respectively.

$$\text{The total OH reactivity} = \sum k_{OH+NMVOC_i}[NMVOC_i] + k_{OH+CH_4}[CH_4] + k_{OH+CO}[CO] + k_{OH+NO}[NO] + k_{OH+NO_2}[NO_2] + k_{OH+SO_2}[SO_2] + k_{OH+O_3}[O_3] + \cdots \quad (1)$$

$$\text{The total } NO_3 \text{ reactivity} = \sum k_{NO_3+NMVOC_i}[NMVOC_i] + k_{NO_3+CH_4}[CH_4] + k_{NO_3+NO}[NO] + k_{NO_3+NO_2}[NO_2] + k_{NO_3+SO_2}[SO_2] + \cdots \quad (2)$$

$$\text{The total } O_3 \text{ reactivity} = \sum k_{O_3+NMVOC_i}[NMVOC_i] + k_{O_3+CH_4}[CH_4] + k_{O_3+NO}[NO] + k_{O_3+NO_2}[NO_2] + \cdots \quad (3)$$

In the above equations, the temperature-dependent reaction rate coefficients (in cm^3 $molecule^{-1}$ s^{-1}) for OH-$NMVOC_i$ ($k_{OH+NMVOC_i}$), OH-CO (k_{OH+CO}), NO_3-$NMVOC_i$ ($k_{NO_3+NMVOC_i}$) and O_3-$NMVOC_i$ ($k_{O_3+NMVOC_i}$) are from Atkinson and Are (2003), Atkinson et al. (2006), Atkinson et al. (1983), Salgado et al. (2008) and the Master Chemical Mechanism, MCM v3.3.1 via the website: http://mcm.leeds.ac.uk/MCM (last accessed: 25 March 2020). OH-NO (k_{OH+NO}), OH-NO_2 (k_{OH+NO_2}), OH-SO_2 (k_{OH+SO_2}), OH-O_3 (k_{OH+O_3}), NO_3-NO (k_{NO_3+NO}), NO_3-NO_2 ($k_{NO_3+NO_2}$),

NO_3-SO_2 ($k_{NO_3+SO_2}$), O_3-NO (k_{O_3+NO}) and O_3-NO_2 ($k_{O_3+NO_2}$) are from Atkinson et al. (2004). The temperature-dependent reaction rate coefficients are listed in Table S1 in the Supplementary Materials. $[NMVOC_i]$, $[CH_4]$, $[CO]$, $[NO]$, $[NO_2]$, $[SO_2]$ and $[O_3]$ are their number concentrations (in molecules cm^{-3}), respectively.

2.5 Atmospheric oxidation capacity

The term "oxidation capacity" of an oxidant X (= NO_3, OH and O_3) is defined as the sum of the respective oxidation rates of the molecules Y_i (NMVOCs, CH_4 and CO) (Geyer et al., 2001).

$$\mathrm{AOC} = \sum_{i=1} k_{Y_i-X}[Y_i]\,[X] = \sum_{i=1} R_X^{Y_i}\,[X] \quad (4)$$

Here, $[Y_i]$ and $[X]$ are number concentrations of molecule Y_i and oxidant X, respectively. k_{Y_i-X} is the temperature-dependent reaction rate coefficients of the molecule Y_i with oxidant X. $R_X^{Y_i}$ is the oxidant X reactivity of molecules Y_i.

2.6 O_3 formation regime

Photochemical formation is the main source of ground-level O_3, and VOCs, CO and NO_x are they key precursors of tropospheric O_3 (Atkinson, 2000). The production of O_3 is generally limited by VOCs or NO_x or by both VOCs and NO_x (Lu et al., 2010; Tang et al., 2012; Li et al., 2019). However, O_3 formation is neither linearly dependent on NO_x concentration nor VOCs reactivity (Pfannerstill et al., 2019); reductions in the emissions of these precursors can decrease, increase, or leave the O_3 production rate unchanged (Pusede and Cohen, 2012). Considering that the impact of VOCs on O_3 formation was more closely related to the reactivity of individual VOC species than to the amount of total VOCs, defining O_3 production regimes in terms of the OH reactivities of VOCs and NOx is also a way of assessing the sensitivity of O_3 production to the prevailing conditions (Kirchner et al., 2001; Lyu et al., 2019; Pfannerstill et al., 2019; Sinha et al., 2012). In this study, we used the relative reactivity (s) of OH towards NO_x and VOCs to evaluate the O_3 production sensitivity, as suggested by Kirchner et al. (2001). The thresholds of the s are 0.2 and 0.01. When $s > 0.2$ it indicates VOC limitation, $0.01<s<0.2$ it is limited by both VOCs and NO_x, and $s < 0.01$ it is limited by NO_x.

3 Results and discussion

3.1 Overview of measurements

For the data evaluation, all measurements were averaged over 1-hour time intervals. The measured concentrations of major pollutants and meteorological parameters at Xianghe are depicted in Figure 2, while the mean diurnal profiles are shown in Figure S1. During the campaign, sunny weather conditions prevailed with temperatures ranging from 25℃ to 31℃ during the daytime. The ambient temperature was comparable with those measured in Beijing (02 Jul-19 Jul 2014), Shanghai (21 Aug-02 Sep 2016), and Chongqing (27 Aug-04 Sep 2015), but higher than that in Guangzhou (23-31 Oct 2015) (Tan et al., 2019). Wind data suggested that the prevailing wind was from the eastern sampling site with a mean wind speed of 1.0 m s^{-1} ranging from 0.3 m s^{-1} to 1.4 m s^{-1}, and the average relative humidity was 85%, reaching up to 96% during the night (Figure 2). For the campaign, NO_y showed a morning peak with a maximum of 228.8 ppb at 9:00 h and an afternoon dip with a minimum of 26.1 ppb at 16:00 h (Figure S1 c). Campaign-averaged data maximum and minimum SO_2 mixing ratios of 3.6 ppb at approximately 14:00 h and 2.3 ppb during nighttime were obtained (Figure S1a). For JO^1D, JNO_2 and JNO_3, a similar maximum at ~14:00 h was observed, with maximum values of 2.1 $\times 10^{-5}$ s^{-1}, 5.3 $\times 10^{-3}$ s^{-1} and 1.3 $\times 10^{-1}$ s^{-1}, respectively (Figure S1k-m). The maximum of JO^1D at this site was comparable with that in Shanghai and Chongqing but higher than that in Guangzhou and lower than that in Beijing (Tan et al., 2019; Wang et al., 2019). The observed mean daily maxima of JNO_2 at this site were higher than those observed in the eastern Mediterranean (Gerasopoulos et al., 2012) but lower than those in Beijing (Wang et al., 2019).

The diurnal maximum O_3 concentration was 72 ppb at this site (Figure S1d), which was in line with that observed in Beijing (72 ppb) but higher than that measured in Guangzhou (65 ppb) and Chongqing (56 ppb) and lower than that observed in Shanghai (80 ppb) (Tan et al., 2019). The O_3 precursors, CO, NO_x, CH_4 and NMVOCs, are shown in Figure 2 and Figure S1. As expected, with the accumulation of CO, NO_x, and NMVOCs, the O_3 concentration gradually increases, and the concentration of NMVOCs gradually decreases as the photochemical reaction progresses (Kansal, 2009; Song et al., 2018). CO and NO_x showed a similar diurnal profile with a maximum during the rush hour and a minimum in the afternoon (Figure S1b and d), suggesting that both CO and NO_x originated from the same source (enhanced traffic emission), and/or were manipulated by the same

factor (e.g., poor dilution conditions). During the campaign, the average mixing ratio of total NMVOCs was 32.4 ppb, with the highest contributions from alkanes (13.2 ppb, 40.6%), followed by OVOCs (12.0 ppb, 37.0%), aromatics (4.3 ppb, 13.2%) and alkenes (3.0 ppb, 9.2%). The top 10 NMVOCs species (Figure 3a), in terms of emissions, consisted of HCHO (7.0 ppb), propane (3.7 ppb), acetone (3.2 ppb), ethane (3.2 ppb), n-butane (1.9 ppb), m/p-xylene (1.6 ppb), iso-pentane (1.3 ppb), ethylene (1.3 ppb), iso-butane (1.1 ppb) and isoprene (1.0 ppb), accounting for 78.4% of the total NMVOCs concentration. As typical tracers of vehicle-related emissions, propane, ethane, ethene, butanes and pentanes were present in high concentrations, suggesting that vehicle-related emissions were likely to be the dominant source of NMVOCs at this site. In addition, the shape of diurnal variations of total NMVOCs backed the presence of vehicle-related emissions, which presented relatively higher mixing ratios during the early morning and from evening to midnight, which may be related to enhanced traffic emissions during rush hours and poor dilution conditions (Yuan et al., 2009; He et al., 2019; Tan et al., 2019). On the other hand, the mixing ratios of total NMVOCs began to decrease at 10:00 h and maintained a broad trough during daytime hours probably due to the increased photochemical removal processes favoring the destruction of NMVOCs, elevated planetary boundary layer (PBL) advancing the dispersion of NMVOCs and/or less NMVOCs emissions reducing levels of NMVOCs (He et al., 2019; Zheng et al., 2018). In contrast, the OVOCs concentrations (Figure S1i) increased from a minimum near sunrise and a maximum in the late afternoon, reflecting the accumulation of OVOCs during the photochemically active period of the day and illustrating the time profile of formation for secondary species (Yuan et al., 2012).

3.2 Reactivities of OH, NO_3 and O_3

3.2.1 OH reactivity

The OH reactivity of trace gases was categorized into SO_2, CO, O_3, NO_x, CH_4 and total NMVOCs, which were grouped into alkanes, alkenes, aromatics and OVOCs (Table S1 lists the NMVOCs included in each group), as shown in Figure 4a and 4b. The total OH reactivity was between 9.2 and 69.6 s^{-1}, with an average of 27.5±9.7 s^{-1} (± standard deviation). Statistically, the average total OH reactivity was much higher than those determined in Beijing (16.4 s^{-1}/20±11 s^{-1}) (Tan et al., 2019; Yang et al., 2017), Shanghai (13.5 s^{-1}) (Tan et al., 2019), Chongqing (17.8 s^{-1})

(Tan et al., 2019), Jinan (19.4±2.1 s^{-1}) (Lyu et al., 2019), Wangdu (10-20 s^{-1}) (Fuchs et al., 2017), Houston (9-22 s^{-1}) (Mao et al., 2010), London (18.1 s^{-1}) (Whalley et al., 2016) and Nashville (11.3 ± 4.8 s^{-1}) (Kovacs et al., 2003), but was comparable or lower than those in Heshan (31±20 s^{-1}) (Yang et al., 2017), Backgarden (mean maximum value of 50 s^{-1}) (Lou et al., 2010) and New York (25 s^{-1}) (Ren et al., 2006b). The OH reactivity towards SO_2, CO and NOx were higher than the values reported in various Chinese cities (Xu et al., 2011; Zhu et al., 2020; Liu et al., 2009) (Table 1). It should be noted that the OH reactivity in this study was calculated from the sum of the products of measured species and their rate coefficients for reactions with OH, and does not involve species that are not measured like monoterpenes and alcohols. Previous studies have showed that there are some discrepancies between the actual measured values and the calculated values of OH reactivity, which may be attributed to missing OH reactivity that originates from VOCs oxidation products of both biogenic and anthropogenic origin (Di Carlo et al., 2004; Dolgorouky et al., 2012; Yoshino et al., 2006; Zhu et al., 2020). Therefore, the OH reactivity calculated in this study is somewhat underestimated.

The total OH reactivity was mainly contributed by NO_x (12.0±7.1 s^{-1}, 43.7%), followed by NMVOCs (7.9±4.8 s^{-1}, 28.5%), CO (7.2±2.6 s^{-1}, 26.0%) and CH_4 (0.3±0.1 s^{-1}, 1.3%) and to a lesser extent by SO_2 and O_3 (0.2±0.1 s^{-1}, 0.6%), indicating the strong influence of anthropogenic emissions in Xianghe. The majority of total OH reactivity values were below 30 s^{-1}, as seen in the frequency distribution, which was dominated by the sum of low OH reactivity contributions and less by single compounds with high OH reactivity (Figure S2a-f), highlighting the necessity of considering a large number of species to obtain a complete picture of total OH reactivity. Specifically, the cumulative frequency distribution (Figure S3a) clearly showed that the OH reactivity at values >40 s^{-1} was dominated entirely by OH reactivity towards NOx, and the OH reactivity at values between 20-40 s^{-1} was nearly dominated by OH reactivity towards NOx and total NMVOCs.

The OH reactivity towards total NMVOCs was 7.9±4.8 s^{-1}, which was much lower than those in Beijing (11.2 s^{-1}) and Heshan (18.3 s^{-1}) (Yang et al., 2017) due to the higher content of reactive hydrocarbons (e.g., alkenes and aromatics) in Beijing and Heshan and due to the unmeasured species (e.g., acetaldehyde) in this study. Alkenes (3.4±3.7 s^{-1}, 42.9%) dominated over OVOCs (2.4±1.5 s^{-1}, 30.2%), aromatics (1.5±1.7 s^{-1}, 18.6%) and alkanes (0.7±0.5 s^{-1}, 8.3%) in the OH reactivity

towards total NMVOCs. The majority of OH reactivity towards total NMVOCs values were below 2 s^{-1} (Figure S4a-d). The cumulative frequency distribution showed that OH reactivity towards total NMVOCs at values of > 6 s^{-1} was dominated by OH reactivity towards alkenes, aromatics and OVOCs, the OH reactivity towards total NMVOCs at values of <6 s^{-1} was dominated by OH reactivity towards alkanes (Figure S5). Alkanes accounted for >50% of the mixing ratio of NMVOCs, but only 8.3% of the OH reactivity towards total NMVOCs. In contrast, aromatics, alkenes and OVOCs accounted for 44.6% of the mixing ratio of NMVOCs, providing 91.7% of the OH reactivity towards total NMVOCs. Significantly, isoprene accounted for only 4% of the mixing ratio of NMVOCs but provided 31.2% of the OH reactivity towards total NMVOCs. This was explained by (1) the relatively low concentration of aromatics, alkenes and OVOCs measured during the campaign, (2) the relatively high concentration of isoprene and (3) the generally large isoprene reaction rate coefficients with OH (101×10^{-12} cm^3 $molecule^{-1}$ s^{-1}) (Atkinson et al., 2006). The top 10 species, in terms of OH reactivity towards total NMVOCs, consisted of isoprene, HCHO, m/p-xylene, ethylene, hexanal, o-xylene, propylene, styrene, methacrolein and cis-2-butene (Figure 3b). These species contributed only 39.1% to NMVOCs emissions but accounted for 80.3% of OH reactivity towards total NMVOCs. As shown in Table 1, OH reactivity towards the speciated NMVOCs in this study were basically within the values reported in various Chinese cities (Tan et al., 2019; Xu et al., 2011; Yang et al., 2017; Zhu et al., 2020).

The mean diurnal profiles of the OH reactivity of trace gases and NMVOCs groups are presented in Figure 5a-f and Figure 6a-d, respectively. In general, the total OH reactivity was the lowest in the afternoon and the highest during rush hours, reaching a maximum of 33.0 s^{-1} during the morning rush hour and a night-time peak of 30.5 s^{-1} (Figure 5a). Most campaigns have also reported a slightly higher OH reactivity in the morning traffic rush hour, which can be explained by higher levels of reactive gases such as NO and NMVOCs due to heavy traffic, as well as slower reactions (Fuchs et al., 2017; Yang et al., 2016). A similar diurnal profile was also observed for contributions from NO_x, CO, alkane and aromatic species, which are typically connected to emissions from anthropogenic activities. The shape of the total OH reactivity diurnal pattern was slightly shifted to the OH reactivity towards NOx strengthening the idea that the local pollution in Xianghe was possibly impacted by traffic emissions. However, a different diurnal behavior to that

of the above species was observed for alkenes (Figure 6b) and OVOCs (Figure 6d), which is emitted by plants or photochemical production. The OH reactivity from OVOCs increased by a factor of approximately 2 from nighttime to daytime, suggesting that during the daytime, dilution or chemical removal had a weaker influence on the observed OVOCs than fresh production by photochemistry. The opposite diurnal variation was reported in Wangdu, which showed a weak diurnal variation with a decrease by a factor of approximately 2 from the morning to the evening (Fuchs et al., 2017). The diurnal profile of OH reactivity towards isoprene appears as the major driver for the diurnal profile of OH reactivity towards alkenes. Biogenic isoprene is dependent on temperature and light intensity (Chang et al., 2014) and anthropogenic isoprene is predominantly emitted by road traffic (Ye et al., 1997); hence, the OH reactivity from alkenes increased during the daytime, with a morning peak of 4.1 s^{-1} at 9:00 h and a night-time peak of 7.4 s^{-1} at 18:00 h. Many rainforest campaigns have also reported a significant diurnal pattern with higher OH reactivity from alkenes and OVOCs at noontime or reached a maximum at the beginning of the night (Yang et al., 2016). Notably, the large amplitude of standard deviation bars highlighted the large diel variability.

3.2.2 NO_3 reactivity

The NO_3 reactivity of trace gases was categorized into SO_2, NO_x, CH_4 and NMVOCs, as shown in Figure 4c and d. Campaign-averaged values of total NO_3 reactivity were 2.2±2.6 s^{-1} ranging from 0.7 s^{-1} to 27.5 s^{-1}. The average total NO_3 reactivity was much higher than those determined during the IBAIRN campaign (Liebmann et al., 2018a) and at a rural mountain site (988 m a.s.l.) in southern Germany in 2017 (Liebmann et al., 2018b) due to the higher contributions from NO_x. We noted that NO_x was by far the main contributors to the total NO_3 reactivity, representing 99% of the total NO_3 reactivity on average. NO exhibited the most prominent contribution to the total NO_3 reactivity and represented an average of 78.0% of the total NO_3 reactivity. In comparison to NO, NO_2 had a maximum contribution during night-time and represented, on average, 27% of the total NO_3 reactivity. The NO_3 reactivity towards CH_4, NMVOCs and SO_2 was very minor, with no more than 1% of the total NO_3 reactivity over the whole campaign. The majority of total NO_3 reactivity values were below 3 s^{-1}, but below 5.5 $\times 10^{-5}$ s^{-1}, 0.1 s^{-1}, 3 s^{-1}, 1×10^{-8} s^{-1} for NO_3 reactivity towards CH_4, total NMVOCs, NOx and SO_2, respectively, as seen in the frequency distribution (Figure S2g-k). The cumulative frequency distribution clearly showed that the total NO_3 reactivity at low and high

values was entirely dominated by NO_3 reactivity towards SO_2 and NOx, respectively (Figure S3b).

The NO_3 reactivity towards total NMVOCs was 2.4±3.0×10^{-2} s^{-1} on average with a minimum of 1.1×10^{-3} s^{-1} and a maximum of 0.3 s^{-1}. The largest fraction of attributed NO_3 reactivity towards total NMVOCs was provided by alkenes (77.8%), followed by aromatics (20.7%) and OVOCs (1.3%). The measured alkanes played virtually no role for NO_3 reactivity towards total NMVOCs, although they accounted for more than 50% of the mixing ratio of NMVOCs. This can be largely explain by the fact that the reaction rate coefficients of alkenes, aromatics and OVOCs with NO_3 are 1-5 orders of magnitude higher than the alkane reaction rate coefficients with NO_3 (Atkinson and Arey, 2003; Atkinson et al., 2006). The majority of NO_3 reactivity towards alkanes, alkenes, aromatics and OVOCs are below 5.0×10^{-5} s^{-1}, 0.1 s^{-1}, 1.0×10^{-2} s^{-1} and 1.0×10^{-3} s^{-1}, respectively (Figure S4e-f). The cumulative frequency distribution showed that NO_3 reactivity towards total NMVOCs at values of > 0.1 s^{-1} was entirely dominated by NO_3 reactivity towards alkenes, the NO_3 reactivity towards total NMVOCs at values between 0.01-0.1 s^{-1} was dominated by NO_3 reactivity towards alkenes and aromatics and the NO_3 reactivity towards total NMVOCs at values of <1.0×10^{-5} s^{-1} was entirely dominated by NO_3 reactivity towards alkanes (Figure S6). The top ten species in terms of NO_3 reactivity towards total NMVOCs consisted of isoprene, styrene, cis-2-butene, trans-2-butene, cis-2-pentene, hexanal, HCHO, propylene, 1,3-butadiene and trans-2-pentene (Figure 3c). These species contributed only 27.7% to NMVOCs emissions but accounted for 99.2% of the NO_3 reactivity towards total NMVOCs.

Total NO_3 reactivity displayed a weak diel variation with a campaign-averaged morning peak value of 4.0s^{-1} at 6:00-7:00 h (Figure 5g). The diurnal profile of NO_3 reactivity towards NOx (Figure 5i) appears to be the major driver for the diurnal profile of total NO_3 reactivity. The morning peak value of total NO_3 reactivity could be explained by the accumulation of NO_x due to traffic emissions that are released into the shallow nocturnal boundary layer during the morning rush hours. In contrast, the average diurnal profile of NO_3 reactivity towards total NMVOCs (Figure 5k) had a maximum at 18:00 h, which was slightly shifted to NO_3 reactivity towards alkenes (Figure 6j). The evening peak value of NO_3 reactivity towards total NMVOCs could be accounted for by the accumulation of alkenes due to vegetation emissions and traffic emissions that are released into the shallow nocturnal boundary layer. NO_3 reactivity towards alkanes (Figure 6e), alkenes (Figure 6f),

aromatics (Figure 6g), OVOCs (Figure 6h) and SO_2 (Figure 5h) played virtually no roles in the diurnal variations of total NO_3 reactivity and NO_3 reactivity towards total NMVOCs, although they exhibited a more distinct diurnal profile.

3.2.3 O_3 reactivity

The O_3 reactivity of trace gases was categorized into NO_x, CH_4 and total NMVOCs, as shown in Figure 4e and f. The total O_3 reactivity at the site varied between a minimum of 3.3×10^{-4} s^{-1} and a maximum of 1.8×10^{-2} s^{-1} and was $1.2\pm1.7\times10^{-3}$ s^{-1} on average. NO exhibited the most prominent contribution to the total O_3 reactivity and represented on average >99% of the total O_3 reactivity, whereas nearly all other contributions were < 1%. This result can be largely accounted for by the generally large NO reaction rate coefficients with O_3 (1.8×10^{-14} cm^3 $molecule^{-1}$ s^{-1}) (Atkinson et al., 2006), which are several orders of magnitude higher than the NO_2, alkanes, alkenes, aromatics and OVOCs reaction rate coefficients with NO_3 (Atkinson et al., 2006; Atkinson and Arey, 2003; Yuan et al., 2013; Ferracci et al., 2018; Jenkin et al., 2015). The majority of total O_3 reactivity values were below 2×10^{-3} s^{-1} but below 5.5×10^{-10} s^{-1}, 2×10^{-6} s^{-1} and 2×10^{-3} s^{-1} for O_3 reactivity towards CH_4, total NMVOCs and NOx, respectively, as seen in the frequency distribution (Figure S2l-o). The cumulative frequency distribution clearly showed that the total O_3 reactivity at low and high values was entirely dominated by O_3 reactivity towards CH_4 and NOx, respectively (Figure S3c).

The O_3 reactivity towards total NMVOCs was $1.1\pm0.8\times10^{-6}$ s^{-1} on average ranging from a minimum of 2.5×10^{-7} s^{-1} to a maximum of 1.0×10^{-5} s^{-1}. Alkenes clearly dominated the O_3 reactivity towards total NMVOCs with campaign-averaged contributions of 94.0%. Aromatics was the second largest contributor, comprising an average of 5.2% of the O_3 reactivity towards total NMVOCs. In comparison, OVOCs only accounted for 0.8% of the O_3 reactivity towards total NMVOCs. In contrast, the measured alkanes played nearly no role for O_3 reactivity towards total NMVOCs due to their small reaction rate coefficients with O_3 (<1.0×10^{-23} cm^3 $molecule^{-1}$ s^{-1}) (Atkinson and Arey, 2003; Atkinson et al., 2006). The majority of O_3 reactivity towards alkanes, alkenes, aromatics and OVOCs were below 5.0×10^{-12} s^{-1}, 3.0×10^{-6} s^{-1}, 2.0×10^{-7} s^{-1} and 2.0×10^{-8} s^{-1}, respectively (Figure S4i-l). The cumulative frequency distribution (Figure S7) clearly showed that the O_3 reactivity towards total NMVOCs at >1.0×10^{-7} s^{-1} was dominated by O_3 reactivity towards alkenes and aromatics, the O_3 reactivity towards total NMVOCs between 1.0×10^{-9} s^{-1} and 1.0×10^{-7} s^{-1} was

dominated by O_3 reactivity towards alkenes, aromatics and OVOCs, and the O_3 reactivity towards NMVOCs <1.0×10^{-11} s^{-1} was entirely dominated by O_3 reactivity towards alkanes. In terms of individual species, isoprene, cis-2-butene, trans-2-butene, cis-2-pentene, propylene, styrene, ethylene, 1-butene, trans-2-pentene and 1-pentene were the top ten species (Figure 3d), accounting for 28%, 25%, 20%, 8%, 7%, 5%, 5%, 3%, 2% and 1%, respectively, of the O_3 reactivity towards total NMVOCs and 3.1%, 0.3%, 0.1%, 0.1%%, 1%, 0.4%, 4.1%, 0.4% 0.1% and 0.1%, respectively, of the total NMVOCs emissions.

Compared with OH and NO_3 reactivities, O_3 reactivity displayed a much weaker diel variation, especially O_3 reactivity towards alkenes and aromatics, as shown in Figure 5 and Figure 6. This can be explained by the following reasons. First, for the same species, the reaction rate coefficients with O_3 were much smaller than its corresponding reaction rate coefficients with OH and NO_3. For example, the ethylene reaction rate coefficients with OH (8.52×10^{-12} cm^3 $molecule^{-1}$ s^{-1}) and NO_3 (2.05×10^{-16} cm^3 $molecule^{-1}$ s^{-1}) are 6 and 2 orders of magnitude higher, respectively, than the ethylene reaction rate coefficients with O_3 (1.59×10^{-18} cm^3 $molecule^{-1}$ s^{-1}) (Atkinson and Arey, 2003; Atkinson et al., 2006). Second, the high-emissions species reaction rate coefficients with O_3 are smaller than the low-emissions species reaction rate coefficients with O_3. For instance, the m/p-xylene (one of the top five emissions species) reaction rate coefficients with O_3 (<1.0×10^{-20} cm^3 $molecule^{-1}$ s^{-1}) are much smaller than the 1-hexene (one of the bottom five emissions species) reaction rate coefficients with O_3 (1.13×10^{-17} cm^3 $molecule^{-1}$ s^{-1}) (Atkinson and Arey, 2003; Atkinson et al., 2006). The above two facets largely weaken the diurnal variation in O_3 reactivity.

3.3 OH reactivity and O_3 production regimes

The O_3 production regime plot (Figure 7) showed that Xianghe was characterized by a strong VOCs limitation. Here, 84% of the datapoints fall within the regime of VOCs limitation, whereas 16% are colimited by both VOCs and NO_x. The higher the O_3 concentration is, the more obvious the VOCs limitation will be. The lower the O_3 concentration is, the more obvious by both VOCs and NO_x will be. Previous studies based on space-based $HCHO/NO_2$ column ratio (Tang et al., 2012) and VOCs / NO_x ratio (Wang et al., 2014) also found that summer O_3 production in this district may be under a VOCs-limited regime. In addition, as VOCs generally have good correlations with CO and play a similar role as CO in photochemical O_3 production (Atkinson, 2000). A scatter plot of

552 CO-NO_y can also be used to evaluate the O_3-NO_x-VOCs sensitivity (Ding et al., 2013). Figure S8
553 depicts the scatter plots of CO-NO_y color-coded with O_3 concentrations. The results showed that
554 high O_3 levels are generally associated with a high CO/NO_y ratio, indicating a VOCs-limited regime
555 of O_3 formation in Xianghe. Generally, our results suggested that control of VOCs would be most
556 effective for controlling O_3 in Xianghe.

557 **3.4 Implications for OH, NO_3 and O_3 reactivities-based NMVOCs control strategies**

558 Table 2 lists the top 10 NMVOCs species (excluding isoprene) in terms of concentrations, OH,
559 NO_3 and O_3 reactivities, and their corresponding contributions to concentrations, OH, NO_3 and O_3
560 reactivities. The order of the major OH, NO_3 and O_3 reactivities-contributing species differed
561 significantly from that of concentration-contributing species. Therefore, NMVOCs control
562 strategies based on OH, NO_3 and O_3 reactivities differ significantly from those based on
563 concentrations.

564 From the perspective of concentrations, HCHO, propane, acetone, ethane, n-butane, m/p-
565 xylene, iso-pentane, ethylene, iso-butane and n-pentane should be targeted. If these 10 species were
566 fully controlled, it would lead to a NMVOCs concentration reduction of 79.9% with only OH, NO_3
567 and O_3 reactivities reductions of 58.4%, 2.1% and 6.4%, respectively. These species are mainly from
568 fuel combustion and vehicle exhaust (Song et al., 2018; Liu et al., 2017); hence from perspective of
569 the current emission-based limits, we recommend that the priorities for the control of NMVOCs
570 sources include fuel combustion and vehicle exhaust.

571 From the perspective of OH reactivity, HCHO, m/p-xylene, ethylene, hexanal, o-xylene,
572 propylene, styrene, methacrolein, cis-butene and methylvinyketone were the key species. If releases
573 of these compounds were reduced to zero without any offset, it would reduce OH reactivity by 73.3%
574 with a NMVOCs concentration reduction of 38.1%, a NO_3 reactivity reduction of 86.4% and O_3
575 reactivity reduction of 55.7%. From the perspective of NO_3 reactivity, the top 10 VOCs species
576 consisted of styrene, cis-2-butene, trans-2-butene, cis-2-pentene, hexanal, HCHO, propylene, 1,3-
577 butadiene, trans-2-pentene and 1-butene. If the concentrations of these species were completely
578 eliminated, it would reduce NO_3 reactivity by 97.8% with a NMVOCs concentration reduction of
579 25.8%, a OH reactivity reduction of 49.7% and a O_3 reactivity reduction of 91.8%. From the
580 perspective of O_3 reactivity, cis-2-butene, trans-2-butene, cis-2-pentene, propylene, styrene,

ethylene, 1-butene, trans-2-pentene, 1-pentene and methacrolein should be key targets for control. If the concentrations of these compounds were reduced to zero without any offset, it would lead to a O_3 reactivity reduction of 98.9% with a VOC concentration reduction of 7.3%, a OH reactivity reduction of 22.3% and a NO_3 reactivity reduction of 94.2%. The top ten species of OH, NO_3 and O_3 reactivities are mainly from traffic-related emissions, industry and solvent usage (Song et al., 2018; Liu et al., 2017; Chen et al., 2014). Therefore, in terms of reactivity-based limits, we recommend that the priorities for the control of NMVOCs sources include traffic-related emissions, industry and solvent usage.

Clearly, species with large concentrations do not necessarily have high OH, NO_3 and O_3 reactivities, and with the least concentration reduction, the maximum reduction of reactivity can be obtained. The key NMVOCs species of OH, NO_3 and O_3 reactivities also differed from each other. However, reducing concentrations of propylene, styrene and cis-2-butene may likely achieve a win-win-win situation. Although the above comparisons were made under the assumption that concentrations would be significantly reduced, it is obvious that OH, NO_3 and O_3 reactivities-based control strategies are more efficient than concentration-based policies in terms of reducing NMVOCs pollution.

3.5 Atmospheric oxidation capacity (AOC)

3.5.1 Modeling OVOCs, OH, HO_2, RO_2 and NO_3 by SOSAA

With the appropriate set up of the condensation sinks for these ten calculated OVOCs (ACR, C_2H_5CHO, MACR, C_3H_7CHO, MVK, MEK, MPRK, C_4H_9CHO, DIEK, $C_5H_{11}CHO$), the modeled diurnal mean pattern generally followed well the measured pattern within the 1 standard deviation of measurement data, although the model underestimated the measurement with less than 1 ppb from 19:00 to 24:00 (Figure S9a). With the inclusion of input MTBE and CH_3COCH_3 (acetone) which constituted more than 50% of the total OVOCs, the modeled total OVOCs concentration agreed better with the measurement than expected (Figure S9b). The modeled diurnal median number concentrations of OH, HO_2 and RO_2 showed an apparent diurnal pattern with peaks during noon while approaching zero during night, which resulted from the dependent of their chemical production reactions on the incoming solar radiation (Figure S10a, b and c). The noon time (12:00-16:00) median values of OH, HO_2 and RO_2 were 1.2×10^7, 5.9×10^8 and 3.7×10^8 molec cm^{-3}, which

were comparable to previous studies (Tan et al., 2017). The diurnal variability of hourly-median NO_3 concentration showed two peaks which were consistent with the high values of the chemical production from $NO_2 + O_3$, which even dominated the photochemical loss of NO_3 (Figure S10d). Figure S11 shows the relationship between modeled OH number concentration and the measured J_O^1D. The coefficient of determination (R^2) was 0.86, and the linear regression fit showed the slope was 6.1×10^{11} cm^{-3} s^{-1} and the intercept was 0.9×10^6 cm^{-3}. These values were comparable to Tan et al. (2017) except the slope was about 36% higher than the observation fit in Tan et al. (2017).

3.5.2 Overall characteristics of AOC

The loss rate of NMVOCs, CH_4 and CO via reactions with OH, O_3 and NO_3 was calculated. The calculated AOC was up to 4.5×10^8 molecules cm^{-3} s^{-1} with campaign-averaged values of 7.8×10^7 molecules cm^{-3} s^{-1}, daytime averages (06:00-18:00 LT) of 1.4×10^8 molecules cm^{-3} s^{-1} and nighttime averages of 6.7×10^6 molecules cm^{-3} s^{-1}. As such, the total number of NMVOCs, CH_4 and CO molecules depleted during daytime and nighttime were 6.0×10^{12} and 2.9×10^{11}, respectively, per cm^{-3} of air. Such AOC levels were higher than those determined at the Tung Chung air quality monitoring station (Xue et al., 2016), from at a polluted area in Santiago, Chile (Elshorbany et al., 2009) and at the Hong Kong Polytechnic University's air monitoring station at Hok Tsui (Li et al., 2018).

Comparisons of calculated AOC by OH, O_3 and NO_3 and corresponding oxidation concentrations are shown in Figure 8. The OH and NO_3 radicals concentrations were simulated by SOSAA box model. The calculated AOC by OH, O_3 and NO_3 corelated well with the corresponding oxidation concentrations, with correlation coefficients (r) of 0.91, 0.83 and 0.57, respectively, suggesting that the parameterized AOC here was consistent with the one obtained using radical concentration to indicate AOC. Specifically, the average oxidation capacities of OH, O_3 and NO_3 radicals throughout the entire campaign were 7.7×10^7, 1.2×10^6 and 1.8×10^5 molecule cm^{-3} s^{-1}, representing 98.2%, 1.5% and 0.3% of the total oxidation capacity, respectively. The total number of depleted molecules per day due to oxidation by OH, O_3 and NO_3 were 6.6×10^{12}, 1.0×10^{11} and 1.5×10^{10} molecules cm^{-3}, respectively, which was slightly higher than that assessed from a polluted area in Santiago, Chile (Elshorbany et al., 2009). Accordingly, the OH radical is the driving force of the oxidation capacity in the atmosphere in Xianghe, especially during daytime. Figure 9 shows

a comparison of the oxidation capacities of OH, O_3 and NO_3. On average, the relative contribution of a 24-hour integral of O_3 and NO_3 oxidation capacity was less than 4% (Figure 9a-c). OH is the only oxidant for CO in the troposphere. As expected, OH was responsible for 99% of the oxidation capacity regarding NMVOCs, CH_4 and CO during the daytime (Figure 9d). The relative contribution of OH initiating oxidation capacity decreased to 98% when restricting the calculation to NMVOCs families alone (Figure 9e). Focusing on the oxidation of unsaturated NMVOCs, OH was the dominant oxidant with a relative proportion of approximately 97% (Figure 9f). Note that the influence of NO_3 and O_3 on the oxidation of CO and VOCs can be neglected during the daytime. However, the elevated relative contributions of O_3 and NO_3 initiating oxidation capacity can be observed during nighttime. As expected, O_3 and NO_3 accounted for 10% and 2%, respectively, of the oxidation capacity regarding NMVOCs, CH_4 and CO (Figure 9g), but 19% and 3% of NMVOCs families alone (Figure 9h) occurred at night. Focusing on the oxidation of unsaturated NMVOCs, O_3 and NO_3 accounted for 20% and 4%, respectively, of the oxidation capacity (Figure 9i). This quantitative intercomparison of the oxidation capacities of OH, O_3 and NO_3 confirms the important role of OH in the degradation of NMVOCs, CH_4 and CO. Compared with OH and O_3, NO_3 had a lower contribution during both the daytime and nighttime, which was mainly caused by the high NO concentrations (Liebmann et al., 2018b).

3.5.3 Relative contributions of NMVOCs oxidation pathways

NMVOCs are mainly consumed by reactions with OH radicals, O_3 and NO_3 radicals in the atmosphere. The time series of NMVOCs loss rates due to the reactions with OH radicals, O_3 and NO_3 radicals are depicted in Figure S12. Diurnal variations of NMVOCs groups and individual species loss rates due to the reactions with different oxidants are shown in Figure 10 and Figure S13-16, respectively. A comparison of the relative contribution of OH, NO_3 and O_3 to the 24 h, daytime and nighttime averaged loss rates is illustrated in Figure S17.

Reactions with OH radicals were the dominant losses for alkanes, accounting for approximately 100% of both daytime and nighttime averaged loss rates of alkanes, respectively. In contrast, reactions with O_3 and NO_3 were nonsignificant for the loss rates of alkanes, accounting for <1% of both the daytime and nighttime averaged loss rates of alkanes. Since alkenes have a greater reaction rate with O_3, oxidation by O_3 also contributes to the loss rates of alkenes. Oxidation by O_3

accounted for 4% of the daytime averaged total loss rate of alkenes. Specifically, the reaction with O_3 was the dominant contributor to nighttime loss rates of trans-2-butene, cis-2-butene and trans-2-pentene, with nighttime contributions of 84.4%, 76.2% and 73.0%, respectively. Reaction oxidation by OH radicals dominated the daytime and nighttime averaged loss rates of the rest of alkenes species. Significantly, in contrast to anthropogenic hydrocarbons, the oxidation by the NO_3 radical is more important for the loss rates of isoprene, contributing to 0.6% and 7.8% of the daytime and nighttime averaged loss rates of isoprene, respectively. For OVOCs species, the reactions with OH radicals were the only significant contributor to their loss rates. Similar to OVOCs species, the reactions with OH radicals were also the only significant contributor to aromatic loss rates, except for styrene, where the reaction with O_3 and NO_3 accounted for 25% and 26%, respectively, of the nighttime averaged loss rates of styrene. In total, oxidation by OH radicals accounted for approximately 100% of the daytime and nighttime averaged loss rates of OVOCs, respectively. Oxidation by OH radicals, NO_3 radicals and O_3 accounted for 90%, 5% and 5%, respectively, of nighttime averaged loss rates of aromatics.

4. Summary and conclusions

In the summer of 2018, a comprehensive field campaign was conducted at a suburban site in the North China Plain. Based on simultaneous measurements of O_3, CO, SO_2, NO, NO_2, JO^1D, JNO_2, JNO_3, HONO, HCHO, CH_4 and 65 NMVOCs, reactivities (OH, NO_3 and O_3 reactivities) for trace gases and atmospheric oxidation capacity (AOC) were comprehensively analyzed. The main findings are summarized as follows.

The total OH reactivity was between 9.2 and 69.6 s^{-1} with an average of 27.5±9.7 s^{-1}, which was mainly contributed by NO_x (43.7%), followed by NMVOCs (28.5%), CO (26.0%) and CH_4 (1.3%) and SO_2 and O_3 (0.5%). OH reactivity towards total NMVOCs was 7.9±4.8 s^{-1} and dominated by alkenes (42.9%). Campaign-averaged values of total NO_3 reactivity were 2.2±2.6 s^{-1}, ranging from 0.7 s^{-1} to 27.5 s^{-1}. NO_x was the main contributors to the total NO_3 reactivity, representing 99% of the total NO_3 reactivity on average. NO_3 reactivity towards total NMVOCs was 2.4±3.0×10^{-2} s^{-1}, on average, and it was dominated by alkenes (77.8%). The total O_3 reactivity varied between a minimum of 3.3×10^{-4} s^{-1} and a maximum of 1.8×10^{-2} s^{-1} with on average of

697 $1.2\pm1.7\times10^{-3}$ s^{-1}. NO exhibited the most prominent contribution to the total O_3 reactivity and
698 represented an average of >99% of the total O_3 reactivity. O_3 reactivity towards total NMVOCs was
699 $1.1\pm0.8\times10^{-6}$ s^{-1} on average, ranging from 2.5×10^{-7} s^{-1} to 1.0×10^{-5} s^{-1} and dominated by alkenes
700 (94.0%). Total OH, NO_3 and O_3 reactivities displayed a similar diel variation with the lowest in the
701 afternoon and the highest during rush hours, and the diurnal profile of NO_x appears to be the major
702 driver for the diurnal profiles of total OH, NO_3 and O_3 reactivities. Compared with OH and NO_3
703 reactivities, O_3 reactivity displayed a much weaker diel variation, especially O_3 reactivity towards
704 alkenes and aromatics due to 1) the rate coefficients with O_3 being much smaller than the
705 corresponding reaction rate coefficients with OH and NO_3 for the same species and 2) the high-
706 emissions species reaction rate coefficients with O_3 being smaller than the low-emissions species
707 reaction rate coefficients with O_3.

708 The relative OH reactivity towards NO_x and VOCs and scatter plots of CO-NO_y color-coded
709 with O_3 concentrations indicated a VOCs-limited regime of O_3 formation in Xianghe, suggesting
710 that control of VOCs would be most effective for controlling O_3 in Xianghe. OH, NO_3 and O_3
711 reactivities-based control strategies are more efficient than concentration-based policies in terms of
712 reducing NMVOCs pollution. We suggest that policy makers shift the current concentration -based
713 limits to reactivity-based policies.

714 The loss rates of NMVOCs, CH_4 and CO via reactions with OH, O_3 and NO_3 were calculated,
715 which were up to 4.5×10^{8} molecules cm^{-3} s^{-1} with campaign-averaged values of 7.8×10^{7} molecules
716 cm^{-3} s^{-1}, daytime averages (06:00-18:00 LT) of 1.4×10^{8} molecules cm^{-3} s^{-1} and nighttime averages
717 of 6.7×10^{6} molecules cm^{-3} s^{-1}. The AOC was dominated by OH radicals (7.7×10^{7} molecule cm^{-3}
718 s^{-1}, 98.2%), O_3 (1.2×10^{6} molecule cm^{-3} s^{-1}, 1.5%) and NO_3 radicals (1.8×10^{5} molecule cm^{-3} s^{-1},
719 0.3%), suggesting that the OH radical is the driving force of the oxidation capacity in the atmosphere
720 in Xianghe, especially during the daytime. The reaction with OH radicals was the dominant loss
721 rates for NMVOCs except for trans-2-butene, cis-2-butene and trans-2-pentene, where the reaction
722 with O_3 was more important for their loss rates during nighttime. Compared with anthropogenic
723 hydrocarbons, the oxidation by NO_3 radical was more important for the nighttime averaged loss
724 rates of isoprene.

725 Our study provides useful insights for VOCs pollution control in a typical suburban site in the

North China Plain. Further studies, especially direct observations of the OH and NO_3 radical, OH and NO_3 reactivity measurements and speciated measurements, are required to further explore the trace gas reactivity and AOC.

Acknowledgement

This study was financially supported by the Ministry of Science and Technology of China (2017YFC0210000), Beijing Major Science and Technology Project (Z181100005418014). All referenced supplemental figures and tables can be found in the supporting information. The authors are grateful to all staff and workers from the Xianghe Atmospheric Observatory of Institute of Atmospheric Physics (IAP) of the Chinese Academy of Sciences for their support during the sampling campaign. We also acknowledge National Meteorological Information Center for providing high quality meteorology parameters. Putian Zhou would also like to acknowledge the University of Helsinki Three Year Grant ("AGES": 2018-2020).

Competing financial interests

The authors declare no competing financial interests.

Author contributions

Y.S.W designed the research. Y.Y and D.Y, S.M.Z, D.S.J, Y.H.W conducted the measurements. Y.Y and Y.H.W interpreted the data and write the paper. P.T.Z and D.C conducted atmospheric chemistry transport model SOSAA simulation. All the authors contributed to discussing results and commenting on the paper.

Reference

Asaf, D., Pedersen, D., Matveev, V., Peleg, M., Kern, C., Zingler, J., Platt, U., and Luria, M.: Long-Term Measurements of NO_3 Radical at a Semiarid Urban Site: 1. Extreme Concentration Events and Their Oxidation Capacity, Environ Sci Technol, 43, 9117-9123, doi:10.1021/es900798b, 2009.

Atkinson, R., Aschmann, S. M., and Jr., J. N. P.: Kinetics of the gas-phase reactions of OH radicals with a series of α,β-unsaturated carbonyls at 299 ± 2 K, International Journal of Chemical Kinetics,

15, 75-81, doi:10.1002/kin.550150108, 1983.

Atkinson, R.: Atmospheric chemistry of VOCs and NOx, Atmos Environ, 34, 2063-2101, doi:10.1016/S1352-2310(99)00460-4, 2000.

Atkinson, R., and Arey, J.: Atmospheric Degradation of Volatile Organic Compounds., Chemical Reviews, 103, 4605-4638, doi:10.102/cr0206420, 2003.

Atkinson, R., Baulch, D. L., Cox, R. A., Crowley, J. N., Hampson, R. F., Hynes, R. G., Jenkin, M. E., Rossi, M. J., and Troe, J.: Evaluated kinetic and photochemical data for atmospheric chemistry: Volume I - gas phase reactions of Ox, HOx, NOx and SOx species, Atmos. Chem. Phys., 4, 1461-1738, doi:10.5194/acp-4-1461-2004, 2004.

Atkinson, R., Baulch, D. L., Cox, R. A., Crowley, J. N., Hampson, R. F., Hynes, R. G., Jenkin, M. E., Rossi, M. J., Troe, J., and IUPAC Subcommittee: Evaluated kinetic and photochemical data for atmospheric chemistry : Volume II - gas phase reactions of organic species, Atmos. Chem. Phys., 6, 3625-4055, doi:10.5194/acp-6-3625-2006, 2006.

Benedict, K. B., Zhou, Y., Sive, B. C., Prenni, A. J., Gebhart, K. A., Fischer, E. V., Evanoski-Cole, A., Sullivan, A. P., Callahan, S., Schichtel, B. A., Mao, H., Zhou, Y., and Collett Jr, J. L.: Volatile Organic Compounds and Ozone in Rocky Mountain National Park during FRAPPÉ, Atmos Chem Phys, 19, 499-521, doi:10.5194/acp-19-499-2019, 2019.

Boy, M., Sogachev, A., Lauros, J., Zhou, L., Guenther, A., and Smolander, S.: SOSA- a new model to simulate the concentrations of organic vapours and sulphuric acid inside the ABL-Part 1: Model description and initial evaluation, Atmos. Chem. Phys., 11, 43-51, doi:10.5194/acp-11-43-2011, 2011.

Carter, W. P. L.: Development of Ozone Reactivity Scales for Volatile Organic Compounds, Air & Waste, 44, 881-899, doi:10.1080/1073161x.1994.10467290, 2012.

Chang, C.-C., Wang, J.-L., Candice Lung, S.-C., Chang, C.-Y., Lee, P.-J., Chew, C., Liao, W.-C., Chen, W.-N., and Ou-Yang, C.-F.: Seasonal characteristics of biogenic and anthropogenic isoprene in tropical-subtropical urban environments, Atmos Environ, 99, 298-308, doi:10.1016/j.atmosenv.2014.09.019, 2014.

Chen, W. T., Shao, M., Lu, S. H., Wang, M., Zeng, L. M., Yuan, B., and Liu, Y.: Understanding primary and secondary sources of ambient carbonyl compounds in Beijing using the PMF model,

784 Atmos Chem Phys, 14, 3047-3062, doi:10.5194/acp-14-3047-2014, 2014.
785 Damian, V., Sandu, A., Damian, M., Potra, F., and Carmichael, G. R.: The kinetic preprocessor KPP-
786 a software environment for solving chemical kinetics, Computers & Chemical Engineering, 26,
787 1567-1579, doi:10.1016/s0098-1354(02)00128-x, 2002.
788 Di Carlo, P., Brune, W. H., Martinez, M., Harder, H., Lesher, R., Ren, X., Thornberry, T., Carroll,
789 M. A., Young, V., Shepson, P. B., Riemer, D., Apel, E., and Campbell, C.: Missing OH reactivity in
790 a forest: evidence for unknown reactive biogenic VOCs, Science, 304, 722-725,
791 doi:10.1126/science.1094392, 2004.
792 Ding, A. J., Fu, C. B., Yang, X. Q., Sun, J. N., Zheng, L. F., Xie, Y. N., Herrmann, E., Nie, W., Petäjä,
793 T., Kerminen, V. M., and Kulmala, M.: Ozone and fine particle in the western Yangtze River Delta:
794 an overview of 1 yr data at the SORPES station, Atmos Chem Phys, 13, 5813-5830,
795 doi:10.5194/acp-13-5813-2013, 2013.
796 Dolgorouky, C., Gros, V., Sarda-Esteve, R., Sinha, V., Williams, J., Marchand, N., Sauvage, S.,
797 Poulain, L., Sciare, J., and Bonsang, B.: Total OH reactivity measurements in Paris during the 2010
798 MEGAPOLI winter campaign, Atmos Chem Phys, 12, 9593-9612, doi:10.5194/acp-12-9593-2012,
799 2012.
800 Elshorbany, Y. F., Kurtenbach, R., Wiesen, P., Lissi, E., Rubio, M., Villena, G., Gramsch, E., Rickard,
801 A. R., Pilling, M. J., and Kleffmann, J.: Oxidation capacity of the city air of Santiago, Chile, Atmos
802 Chem Phys, 9, 2257-2273, doi:10.5194/acp-9-2257-2009, 2009.
803 Elshorbany, Y. F., Kleffmann, J., Hofzumahaus, A., Kurtenbach, R., Wiesen, P., Brauers, T., Bohn,
804 B., Dorn, H. P., Fuchs, H., Holland, F., Rohrer, F., Tillmann, R., Wegener, R., Wahner, A., Kanaya,
805 Y., Yoshino, A., Nishida, S., Kajii, Y., Martinez, M., Kubistin, D., Harder, H., Lelieveld, J., Elste, T.,
806 Plass-Dülmer, C., Stange, G., Berresheim, H., and Schurath, U.: HOx budgets during HOxComp: A
807 case study of HOx chemistry under NOx-limited conditions, Journal of Geophysical Research:
808 Atmospheres, 117, doi:10.1029/2011jd017008, 2012.
809 Ferracci, V., Heimann, I., Abraham, N. L., Pyle, J. A., and Archibald, A. T.: Global modelling of the
810 total OH reactivity: investigations on the “missing” OH sink and its atmospheric implications,
811 Atmos Chem Phys, 18, 7109-7129, doi:10.5194/acp-18-7109-2018, 2018.
812 Fuchs, H., Tan, Z., Lu, K., Bohn, B., Broch, S., Brown, S. S., Dong, H., Gomm, S., Häseler, R., He,

L., Hofzumahaus, A., Holland, F., Li, X., Liu, Y., Lu, S., Min, K.-E., Rohrer, F., Shao, M., Wang, B., Wang, M., Wu, Y., Zeng, L., Zhang, Y., Wahner, A., and Zhang, Y.: OH reactivity at a rural site (Wangdu) in the North China Plain: contributions from OH reactants and experimental OH budget, Atmos Chem Phys, 17, 645-661, doi:10.5194/acp-17-645-2017, 2017.

Gerasopoulos, E., Kazadzis, S., Vrekoussis, M., Kouvarakis, G., Liakakou, E., Kouremeti, N., Giannadaki, D., Kanakidou, M., Bohn, B., and Mihalopoulos, N.: Factors affecting O_3 and NO_2 photolysis frequencies measured in the eastern Mediterranean during the five-year period 2002-2006, Journal of Geophysical Research: Atmospheres, 117, doi:10.1029/2012jd017622, 2012.

Geyer, A., Alicke, B., Konrad, S., Schmitz, T., Stutz, J., and Platt, U.: Chemistry and oxidation capacity of the nitrate radical in the continental boundary layer near Berlin, Journal of Geophysical Research: Atmospheres, 106, 8013-8025, doi:10.1029/2000jd900681, 2001.

Geyer, A.: Nighttime formation of peroxy and hydroxyl radicals during the BERLIOZ campaign: Observations and modeling studies, Journal of Geophysical Research, 108, doi:10.1029/2001jd000656, 2003.

Goldan, P. D., Kuster, W. C., Williams, E., Murphy, P. C., Fehsenfeld, F. C., and Meagher, J.: Nonmethane hydrocarbon and oxy hydrocarbon measurements during the 2002 New England Air Quality Study, Journal of Geophysical Research: Atmospheres, 109, D21309, doi:10.1029/2003jd004455, 2004.

Goldstein, A. H., and Galbally, I. E.: Known and unexplored organic constituents in the earth's atmosphere, Environ Sci Technol, 41, 1514-1521, doi:10.1021/es072476p, 2007.

He, Z., Wang, X., Ling, Z., Zhao, J., Guo, H., Shao, M., and Wang, Z.: Contributions of different anthropogenic volatile organic compound sources to ozone formation at a receptor site in the Pearl River Delta region and its policy implications, Atmos. Chem. Phys., 19, 8801-8816, doi:10.5194/acp-19-8801-2019, 2019.

Heard, D. E., and Pilling, M. J.: Measurement of OH and HO_2 in the troposphere, Chemical Reviews, 103, 5163-5198, doi:10.1021/cr020522s, 2003.

Jenkin, M. E., Saunders, S. M., and Pilling, M. J.: The tropospheric degradation of volatile organic compounds: a protocol for mechanism development, Atmos Environ, 31, 81-104, doi:10.1016/S1352-2310(96)00105-7, 1997.

842 Jenkin, M. E., Young, J. C., and Rickard, A. R.: The MCM v3.3.1 degradation scheme for isoprene,
843 Atmos. Chem. Phys., 15, 11433-11459, doi:10.5194/acp-15-11433-2015, 2015.
844 Kaiser, J., Wolfe, G. M., Bohn, B., Broch, S., Fuchs, H., Ganzeveld, L. N., Gomm, S., Häseler, R.,
845 Hofzumahaus, A., Holland, F., Jäger, J., Li, X., Lohse, I., Lu, K., Prévôt, A. S. H., Rohrer, F.,
846 Wegener, R., Wolf, R., Mentel, T. F., Kiendler-Scharr, A., Wahner, A., and Keutsch, F. N.: Evidence
847 for an unidentified non-photochemical ground-level source of formaldehyde in the Po Valley with
848 potential implications for ozone production, Atmos. Chem. Phys., 15, 1289-1298, doi:10.5194/acp-
849 15-1289-2015, 2015.
850 Kansal, A.: Sources and reactivity of NMHCs and VOCs in the atmosphere: a review, J Hazard
851 Mater, 166, 17-26, doi:10.1016/j.jhazmat.2008.11.048, 2009.
852 Kim, S., Sanchez, D., Wang, M., Seco, R., Jeong, D., Hughes, S., Barletta, B., Blake, D. R., Jung,
853 J., Kim, D., Lee, G., Lee, M., Ahn, J., Lee, S. D., Cho, G., Sung, M. Y., Lee, Y. H., Kim, D. B., Kim,
854 Y., Woo, J. H., Jo, D., Park, R., Park, J. H., Hong, Y. D., and Hong, J. H.: OH reactivity in urban and
855 suburban regions in Seoul, South Korea - an East Asian megacity in a rapid transition, Faraday
856 Discuss, 189, 231-251, doi:10.1039/c5fd00230c, 2016.
857 Kirchner, F., Jeanneret, F., Clappier, A., Krüger, B., van den Bergh, H., and Calpini, B.: Total VOC
858 reactivity in the planetary boundary layer: 2. A new indicator for determining the sensitivity of the
859 ozone production to VOC and NOx, Journal of Geophysical Research: Atmospheres, 106, 3095-
860 3110, doi:10.1029/2000jd900603, 2001.
861 Kovacs, T. A., Brune, W. H., Harder, H., Martinez, M., Simpas, J. B., Frost, G. J., Williams, E.,
862 Jobson, T., Stroud, C., Young, V., Fried, A., and Wert, B.: Direct measurements of urban OH
863 reactivity during Nashville SOS in summer 1999, J Environ Monitor, 5, 68-74,
864 doi:10.1039/b204339d, 2003.
865 Kumar, V., Chandra, B. P., and Sinha, V.: Large unexplained suite of chemically reactive compounds
866 present in ambient air due to biomass fires, Sci Rep-Uk, 8, 626, doi:10.1038/s41598-017-19139-3,
867 2018.
868 Lee, J. D., Young, J. C., Read, K. A., Hamilton, J. F., Hopkins, J. R., Lewis, A. C., Bandy, B. J.,
869 Davey, J., Edwards, P., Ingham, T., Self, D. E., Smith, S. C., Pilling, M. J., and Heard, D. E.:
870 Measurement and calculation of OH reactivity at a United Kingdom coastal site, J Atmos Chem, 64,

53-76, doi:10.1007/s10874-010-9171-0, 2010.

Li, K., Jacob, D. J., Liao, H., Shen, L., Zhang, Q., and Bates, K. H.: Anthropogenic drivers of 2013-2017 trends in summer surface ozone in China, Proc Natl Acad Sci US A, 116, 422-427, doi:10.1073/pnas.1812168116, 2019.

Li, Z., Xue, L., Yang, X., Zha, Q., Tham, Y. J., Yan, C., Louie, P. K. K., Luk, C. W. Y., Wang, T., and Wang, W.: Oxidizing capacity of the rural atmosphere in Hong Kong, Southern China, Sci Total Environ, 612, 1114-1122, doi:10.1016/j.scitotenv.2017.08.310, 2018.

Liebmann, J., Karu, E., Sobanski, N., Schuladen, J., Ehn, M., Schallhart, S., Quéléver, L., Hellen, H., Hakola, H., Hoffmann, T., Williams, J., Fischer, H., Lelieveld, J., and Crowley, J. N.: Direct measurement of NO_3 radical reactivity in a boreal forest, Atmos Chem Phys, 18, 3799-3815, doi:10.5194/acp-18-3799-2018, 2018a.

Liebmann, J. M., Schuster, G., Schuladen, J. B., Sobanski, N., Lelieveld, J., and Crowley, J. N.: Measurement of ambient NO_3 reactivity: design, characterization and first deployment of a new instrument, Atmos Meas Tech, 10, 1241-1258, doi:10.5194/amt-10-1241-2017, 2017.

Liebmann, J. M., Muller, J. B. A., Kubistin, D., Claude, A., Holla, R., Plass-Dülmer, C., Lelieveld, J., and Crowley, J. N.: Direct measurements of NO_3 reactivity in and above the boundary layer of a mountaintop site: identification of reactive trace gases and comparison with OH reactivity, Atmos Chem Phys, 18, 12045-12059, doi:10.5194/acp-18-12045-2018, 2018b.

Liu, C. T., Ma, Z. B., Mu, Y. J., Liu, J. F., Zhang, C. L., Zhang, Y. Y., Liu, P. F., and Zhang, H. X.: The levels, variation characteristics, and sources of atmospheric non-methane hydrocarbon compounds during wintertime in Beijing, China, Atmos Chem Phys, 17, 10633-10649, doi:10.5194/acp-17-10633-2017, 2017.

Liu, Y., Shao, M., Lu, S. H., Liao, C. C., Wang, J. L., and Chen, G.: Volatile organic compound (VOC) measurements in the pearl river delta (PRD) region, China, Atmos Chem Phys, 8, 1531-1545, doi:10.5194/acp-8-1531-2008, 2008.

Liu, Y., Shao, M., Kuster, W. C., Goldan, P. D., Li, X., Lu, S., and de Gouw, J. A.: Source identification of reactive hydrocarbons and oxygenated VOCs in the summertime in Beijing, Environ Sci Technol, 43, 75-81, doi:10.1021/es801716n, 2009.

Lou, S., Holland, F., Rohrer, F., Lu, K., Bohn, B., Brauers, T., Chang, C. C., Fuchs, H., Häseler, R.,

Kita, K., Kondo, Y., Li, X., Shao, M., Zeng, L., Wahner, A., Zhang, Y., Wang, W., and Hofzumahaus, A.: Atmospheric OH reactivities in the Pearl River Delta – China in summer 2006: measurement and model results, Atmos Chem Phys, 10, 11243-11260, doi:10.5194/acp-10-11243-2010, 2010.

Lu, K., Zhang, Y., Su, H., Brauers, T., Chou, C. C., Hofzumahaus, A., Liu, S. C., Kita, K., Kondo, Y., Shao, M., Wahner, A., Wang, J., Wang, X., and Zhu, T.: Oxidant (O_3+ NO_2) production processes and formation regimes in Beijing, Journal of Geophysical Research, 115, doi:10.1029/2009jd012714, 2010.

Lu, K., Guo, S., Tan, Z., Wang, H., Shang, D., Liu, Y., Li, X., Wu, Z., Hu, M., and Zhang, Y.: Exploring the Atmospheric Free Radical chemistry in China: The Self-Cleansing Capacity and the Formation of Secondary air Pollution, National Science Review, doi:10.1093/nsr/nwy073, 2018.

Lu, K., Fuchs, H., Hofzumahaus, A., Tan, Z., Wang, H., Zhang, L., Schmitt, S. H., Rohrer, F., Bohn, B., Broch, S., Dong, H., Gkatzelis, G. I., Hohaus, T., Holland, F., Li, X., Liu, Y., Liu, Y., Ma, X., Novelli, A., Schlag, P., Shao, M., Wu, Y., Wu, Z., Zeng, L., Hu, M., Kiendler-Scharr, A., Wahner, A., and Zhang, Y.: Fast Photochemistry in Wintertime Haze: Consequences for Pollution Mitigation Strategies, Environ Sci Technol, 53, 10676-10684, doi:10.1021/acs.est.9b02422, 2019.

Lu, K. D., Hofzumahaus, A., Holland, F., Bohn, B., Brauers, T., Fuchs, H., Hu, M., Häseler, R., Kita, K., Kondo, Y., Li, X., Lou, S. R., Oebel, A., Shao, M., Zeng, L. M., Wahner, A., Zhu, T., Zhang, Y. H., and Rohrer, F.: Missing OH source in a suburban environment near Beijing: observed and modelled OH and HO_2 concentrations in summer 2006, Atmos. Chem. Phys., 13, 1057-1080, doi:10.5194/acp-13-1057-2013, 2013.

Lyu, X., Wang, N., Guo, H., Xue, L., Jiang, F., Zeren, Y., Cheng, H., Cai, Z., Han, L., and Zhou, Y.: Causes of a continuous summertime O_3 pollution event in Jinan, a central city in the North China Plain, Atmos Chem Phys, 19, 3025-3042, doi:10.5194/acp-19-3025-2019, 2019.

Mao, J., Ren, X., Chen, S., Brune, W. H., Chen, Z., Martinez, M., Harder, H., Lefer, B., Rappenglück, B., Flynn, J., and Leuchner, M.: Atmospheric oxidation capacity in the summer of Houston 2006: Comparison with summer measurements in other metropolitan studies, Atmos Environ, 44, 4107-4115, doi:10.1016/j.atmosenv.2009.01.013, 2010.

Mogensen, D., Smolander, S., Sogachev, A., Zhou, L., Sinha, V., Guenther, A., Williams, J., Nieminen, T., Kajos, M. K., and Rinne, J.: Modelling atmospheric OH-reactivity in a boreal forest

ecosystem, Atmospheric Chemistry & Physics, 11, 9709-9719, doi:10.5194/acp-11-9709-2011, 2011.

Mogensen, D., Gierens, R., Crowley, J. N., Keronen, P., and Smolander, S.: Simulations of atmospheric OH, O_3 and NO_3 reactivities within and above the boreal forest, Atmospheric Chemistry & Physics, 15, 3909-3932, doi:10.5194/acp-15-3909-2015, 2015.

Pfannerstill, E. Y., Wang, N. J., Edtbauer, A., Bourtsoukidis, E., Crowley, J. N., Dienhart, D., Eger, P. G., Ernle, L., Fischer, H., Hottmann, B., Paris, J. D., Stonner, C., Tadic, I., Walter, D., and Williams, J.: Shipborne measurements of total OH reactivity around the Arabian Peninsula and its role in ozone chemistry, Atmos Chem Phys, 19, 11501-11523, doi:10.5194/acp-19-11501-2019, 2019.

Praplan, A. P., Pfannerstill, E. Y., Williams, J., and Hellén, H.: OH reactivity of the urban air in Helsinki, Finland, during winter, Atmos Environ, 169, 150-161, doi:10.1016/j.atmosenv.2017.09.013, 2017.

Pusede, S. E., and Cohen, R. C.: On the observed response of ozone to NOx and VOC reactivity reductions in San Joaquin Valley California 1995–present, Atmos Chem Phys, 12, 8323-8339, doi:10.5194/acp-12-8323-2012, 2012.

Ren, X.: HOx concentrations and OH reactivity observations in New York City during PMTACS-NY2001, Atmos Environ, 37, 3627-3637, doi:10.1016/s1352-2310(03)00460-6, 2003.

Ren, X., Brune, W. H., Mao, J., Mitchell, M. J., Lesher, R. L., Simpas, J. B., Metcalf, A. R., Schwab, J. J., Cai, C., and Li, Y.: Behavior of OH and HO_2 in the winter atmosphere in New York City, Atmos Environ, 40, 252-263, doi:10.1016/j.atmosenv.2005.11.073, 2006a.

Ren, X., Brune, W. H., Oliger, A., Metcalf, A. R., Simpas, J. B., Shirley, T., Schwab, J. J., Bai, C., Roychowdhury, U., Li, Y., Cai, C., Demerjian, K. L., He, Y., Zhou, X., Gao, H., and Hou, J.: OH, HO_2, and OH reactivity during the PMTACS-NY Whiteface Mountain 2002 campaign: Observations and model comparison, Journal of Geophysical Research: Atmospheres, 111, doi:10.1029/2005jd006126, 2006b.

Sadanaga, Y., Yoshino, A., Kato, S., and Kajii, Y.: Measurements of OH reactivity and photochemical ozone production in the urban atmosphere, Environ Sci Technol, 39, 8847-8852, doi:10.1021/es049457p, 2005.

Salgado, M. S., Monedero, E., Villanueva, F., Martín, P., Tapia, A., and Caba?as, B.: Night-Time Atmospheric Fate of Acrolein and Crotonaldehyde, Environ Sci Technol, 42, 2394-2400, doi:10.1021/es702533u, 2008.

Saunders, S. M., Jenkin, M. E., Derwent, R. G., and Pilling, M. J.: Protocol for the development of the Master Chemical Mechanism, MCM v3 (Part A): tropospheric degradation of non-aromatic volatile organic compounds, Atmos. Chem. Phys., 3, 161-180, doi:10.5194/acp-3-161-2003, 2003.

Shirley, T. R., Brune, W. H., Ren, X., Mao, J., Lesher, R., Cardenas, B., Volkamer, R., Molina, L. T., Molina, M. J., Lamb, B., Velasco, E., Jobson, T., and Alexander, M.: Atmospheric oxidation in the Mexico City Metropolitan Area (MCMA) during April 2003, Atmos Chem Phys, 6, 2753-2765, doi:10.5194/acp-6-2753-2006, 2006.

Sinha, V., Williams, J., Crowley, J. N., and Lelieveld, J.: The Comparative Reactivity Method – a new tool to measure total OH Reactivity in ambient air, Atmos. Chem. Phys., 8, 2213-2227, doi:10.5194/acp-8-2213-2008, 2008.

Sinha, V., Williams, J., Diesch, J. M., Drewnick, F., Martinez, M., Harder, H., Regelin, E., Kubistin, D., Bozem, H., Hosaynali-Beygi, Z., Fischer, H., Andrés-Hernández, M. D., Kartal, D., Adame, J. A., and Lelieveld, J.: Constraints on instantaneous ozone production rates and regimes during DOMINO derived using in-situ OH reactivity measurements, Atmos Chem Phys, 12, 7269-7283, doi:10.5194/acp-12-7269-2012, 2012.

Song, M. D., Tan, Q. W., Feng, M., Qu, Y., Liu, X. G., An, J. L., and Zhang, Y. H.: Source Apportionment and Secondary Transformation of Atmospheric Nonmethane Hydrocarbons in Chengdu, Southwest China, J Geophys Res-Atmos, 123, 9741-9763, doi:10.1029/2018jd028479, 2018.

Tan, Z., Fuchs, H., Lu, K., Hofzumahaus, A., Bohn, B., Broch, S., Dong, H., Gomm, S., Häseler, R., He, L., Holland, F., Li, X., Liu, Y., Lu, S., Rohrer, F., Shao, M., Wang, B., Wang, M., Wu, Y., Zeng, L., Zhang, Y., Wahner, A., and Zhang, Y.: Radical chemistry at a rural site (Wangdu) in the North China Plain: observation and model calculations of OH, HO_2 and RO_2 radicals, Atmos. Chem. Phys., 17, 663-690, doi:10.5194/acp-17-663-2017, 2017.

Tan, Z., Lu, K., Jiang, M., Su, R., Wang, H., Lou, S., Fu, Q., Zhai, C., Tan, Q., Yue, D., Chen, D., Wang, Z., Xie, S., Zeng, L., and Zhang, Y.: Daytime atmospheric oxidation capacity in four Chinese

megacities during the photochemically polluted season: a case study based on box model simulation, Atmos Chem Phys, 19, 3493-3513, doi:10.5194/acp-19-3493-2019, 2019.

Tang, G., Wang, Y., Li, X., Ji, D., Hsu, S., and Gao, X.: Spatial-temporal variations in surface ozone in Northern China as observed during 2009–2010 and possible implications for future air quality control strategies, Atmos Chem Phys, 12, 2757-2776, doi:10.5194/acp-12-2757-2012, 2012.

Tong, S., Hou, S., Zhang, Y., Chu, B., Liu, Y., He, H., Zhao, P., and Ge, M.-F.: Exploring the nitrous acid (HONO) formation mechanism in winter Beijing: direct emissions and heterogeneous production in urban and suburban areas, Faraday Discuss., 189, doi:10.1039/C5FD00163C, 2015.

Wang, W., Li, X., Shao, M., Hu, M., Zeng, L., Wu, Y., and Tan, T.: The impact of aerosols on photolysis frequencies and ozone production in Beijing during the 4-year period 2012–2015, Atmos Chem Phys, 19, 9413-9429, doi:10.5194/acp-19-9413-2019, 2019.

Wang, Y., Hu, B., Tang, G., Ji, D., Zhang, H., Bai, J., Wang, X., and Wang, Y.: Characteristics of ozone and its precursors in Northern China: A comparative study of three sites, Atmos Res, 132-133, 450-459, doi:10.1016/j.atmosres.2013.04.005, 2013.

Wang, Y. H., Hu, B., Ji, D. S., Liu, Z. R., Tang, G. Q., Xin, J. Y., Zhang, H. X., Song, T., Wang, L. L., Gao, W. K., Wang, X. K., and Wang, Y. S.: Ozone weekend effects in the Beijing–Tianjin–Hebei metropolitan area, China, Atmos Chem Phys, 14, 2419-2429, doi:10.5194/acp-14-2419-2014, 2014.

Warneke, C.: Comparison of daytime and nighttime oxidation of biogenic and anthropogenic VOCs along the New England coast in summer during New England Air Quality Study 2002, Journal of Geophysical Research, 109, D10309, doi:10.1029/2003jd004424, 2004.

Whalley, L. K., Stone, D., Bandy, B., Dunmore, R., Hamilton, J. F., Hopkins, J., Lee, J. D., Lewis, A. C., and Heard, D. E.: Atmospheric OH reactivity in central London: observations, model predictions and estimates of in situ ozone production, Atmos Chem Phys, 16, 2109-2122, doi:10.5194/acp-16-2109-2016, 2016.

Williams, J., Keßel, S. U., Nölscher, A. C., Yang, Y., Lee, Y., Yáñez-Serrano, A. M., Wolff, S., Kesselmeier, J., Klüpfel, T., Lelieveld, J., and Shao, M.: Opposite OH reactivity and ozone cycles in the Amazon rainforest and megacity Beijing: Subversion of biospheric oxidant control by anthropogenic emissions, Atmos Environ, 125, 112-118, doi:10.1016/j.atmosenv.2015.11.007, 2016.

Wu, R., Li, J., Hao, Y., Li, Y., Zeng, L., and Xie, S.: Evolution process and sources of ambient

volatile organic compounds during a severe haze event in Beijing, China, Sci Total Environ, 560-561, 62-72, doi:10.1016/j.scitotenv.2016.04.030, 2016.

Xin, J. Y., Wang, Y. S., Tang, G. Q., Wang, L. L., Sun, Y., Wang, Y. H., Hu, B., Song, T., Ji, D. S., and Wang, W. F.: Variability and reduction of atmospheric pollutants in Beijing and its surrounding area during the Beijing 2008 Olympic Games, Chinese Sci Bull, 55, 1937-1944, doi: 10.1007/s00376-012-1227-4, 2012.

Xu, J., Ma, J. Z., Zhang, X. L., Xu, X. B., Xu, X. F., Lin, W. L., Wang, Y., Meng, W., and Ma, Z. Q.: Measurements of ozone and its precursors in Beijing during summertime: impact of urban plumes on ozone pollution in downwind rural areas, Atmos Chem Phys, 11, 12241-12252, doi:10.5194/acp-11-12241-2011, 2011.

Xue, L., Gu, R., Wang, T., Wang, X., Saunders, S., Blake, D., Louie, P. K. K., Luk, C. W. Y., Simpson, I., Xu, Z., Wang, Z., Gao, Y., Lee, S., Mellouki, A., and Wang, W.: Oxidative capacity and radical chemistry in the polluted atmosphere of Hong Kong and Pearl River Delta region: analysis of a severe photochemical smog episode, Atmos Chem Phys, 16, 9891-9903, doi:10.5194/acp-16-9891-2016, 2016.

Yang, Y., Shao, M., Wang, X., Nölscher, A. C., Kessel, S., Guenther, A., and Williams, J.: Towards a quantitative understanding of total OH reactivity: A review, Atmos Environ, 134, 147-161, doi:10.1016/j.atmosenv.2016.03.010, 2016.

Yang, Y., Shao, M., Keßel, S., Li, Y., Lu, K., Lu, S., Williams, J., Zhang, Y., Zeng, L., Nölscher, A. C., Wu, Y., Wang, X., and Zheng, J.: How the OH reactivity affects the ozone production efficiency: case studies in Beijing and Heshan, China, Atmos Chem Phys, 17, 7127-7142, doi:10.5194/acp-17-7127-2017, 2017.

Yang, Y., Ji, D., Sun, J., Wang, Y., Yao, D., Zhao, S., Yu, X., Zeng, L., Zhang, R., Zhang, H., Wang, Y., and Wang, Y.: Ambient volatile organic compounds in a suburban site between Beijing and Tianjin: Concentration levels, source apportionment and health risk assessment, Sci Total Environ, 695, 133889, doi:10.1016/j.scitotenv.2019.133889, 2019.

Ye, Y., Galbally, I., and Weeks, I.: Emission of 1,3-butadiene from petrol-driven motor vehicles, Atmos Environ, 31, 1157-1165, doi:10.1016/S1352-2310(96)00308-1, 1997.

Yoshino, A., Sadanaga, Y., Watanabe, K., Kato, S., Miyakawa, Y., Matsumoto, J., and Kajii, Y.:

Measurement of total OH reactivity by laser-induced pump and probe technique—comprehensive observations in the urban atmosphere of Tokyo, Atmos Environ, 40, 7869-7881, doi:10.1016/j.atmosenv.2006.07.023, 2006.

Yuan, B., Shao, M., de Gouw, J., Parrish, D. D., Lu, S., Wang, M., Zeng, L., Zhang, Q., Song, Y., Zhang, J., and Hu, M.: Volatile organic compounds (VOCs) in urban air: How chemistry affects the interpretation of positive matrix factorization (PMF) analysis, Journal of Geophysical Research: Atmospheres, 117, 24302, doi:10.1029/2012jd018236, 2012.

Yuan, B., Hu, W. W., Shao, M., Wang, M., Chen, W. T., Lu, S. H., Zeng, L. M., and Hu, M.: VOC emissions, evolutions and contributions to SOA formation at a receptor site in eastern China, Atmos Chem Phys, 13, 8815-8832, doi:10.5194/acp-13-8815-2013, 2013.

Yuan, Z. B., Lau, A. K. H., Shao, M., Louie, P. K. K., Liu, S. C., and Zhu, T.: Source analysis of volatile organic compounds by positive matrix factorization in urban and rural environments in Beijing, J Geophys Res-Atmos, 114, doi:10.1029/2008JD011190, 2009.

Zannoni, N., Gros, V., Sarda Esteve, R., Kalogridis, C., Michoud, V., Dusanter, S., Sauvage, S., Locoge, N., Colomb, A., and Bonsang, B.: Summertime OH reactivity from a receptor coastal site in the Mediterranean Basin, Atmos Chem Phys, 17, 12645-12658, doi:10.5194/acp-17-12645-2017, 2017.

Zhang, W., Tong, S., Ge, M.-F., An, J., Shi, Z., Hou, S., Xia, K., qu, y., Zhang, H., Chu, B., Sun, Y., and He, H.: Variations and sources of nitrous acid (HONO) during a severe pollution episode in Beijing in winter 2016, Sci Total Environ, 648, doi:10.1016/j.scitotenv.2018.08.133, 2019.

Zheng, H., Kong, S. F., Xing, X. L., Mao, Y., Hu, T. P., Ding, Y., Li, G., Liu, D. T., Li, S. L., and Qi, S. H.: Monitoring of volatile organic compounds (VOCs) from an oil and gas station in northwest China for 1 year, Atmos Chem Phys, 18, 4567-4595, doi:10.5194/acp-18-4567-2018, 2018.

Zhou, P., Ganzeveld, L., Rannik, ü., Zhou, L., Gierens, R., Taipale, D., Mammarella, I., and Boy, M.: Simulating ozone dry deposition at a boreal forest with a multi-layer canopy deposition model, Atmospheric Chemistry & Physics, 17, 1361-1379, doi:10.5194/acp-17-1361-2017, 2017a.

Zhou, P., Ganzeveld, L., Taipale, D., Rannik, Ü., Rantala, P., Rissanen, M. P., Chen, D., and Boy, M.: Boreal forest BVOC exchange: emissions versus in-canopy sinks, Atmos. Chem. Phys., 17, 14309-14332, doi:10.5194/acp-17-14309-2017, 2017b.

Zhu, J., Wang, S., Wang, H., Jing, S., Lou, S., Saiz-Lopez, A., and Zhou, B.: Observationally constrained modeling of atmospheric oxidation capacity and photochemical reactivity in Shanghai, China, Atmos. Chem. Phys., 20, 1217-1232, doi:10.5194/acp-20-1217-2020, 2020.

Figure captions

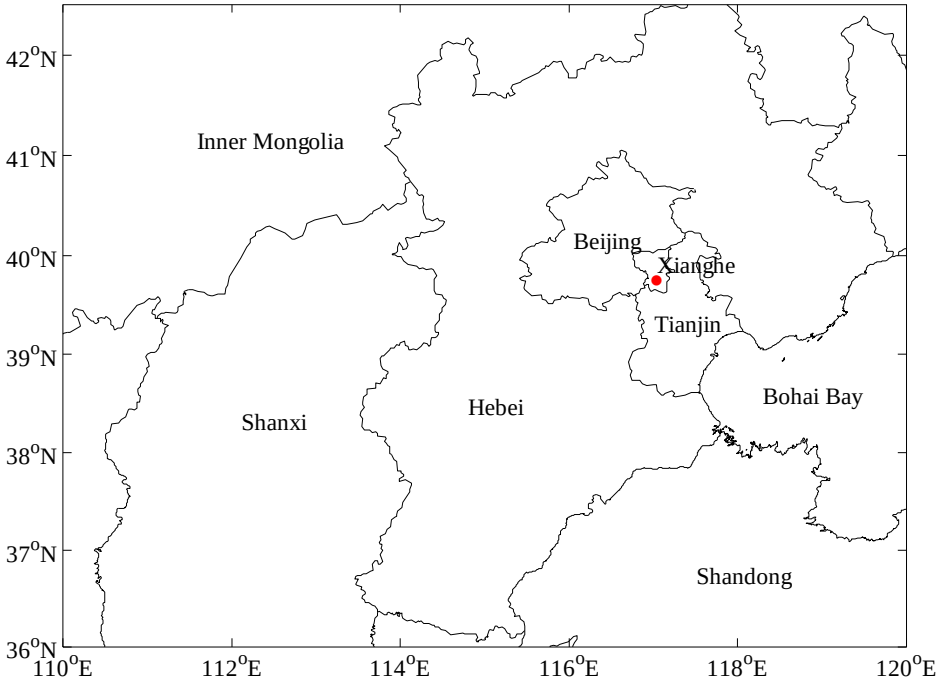

Figure 1. The location of the sampling site, which is marked with a red dot. The blacklines are provincial boundary lines of each province. (The figure was produced by MATLAB 2017a).

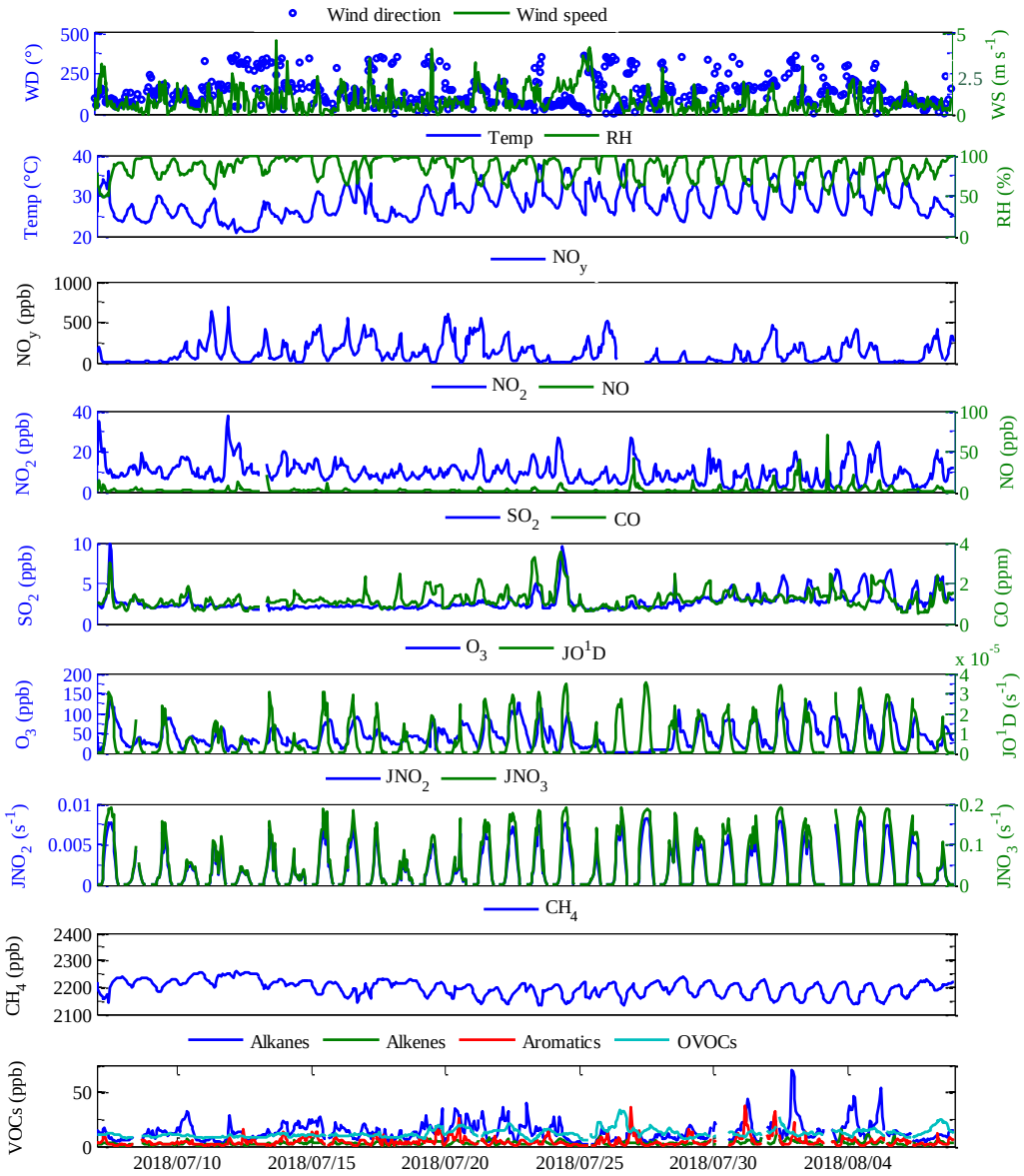

Figure 2. Time series of meteorology parameters, trace gases, photolysis rates and VOCs concentrations during the field campaign at Xianghe from 6 July to 6 August 2018.

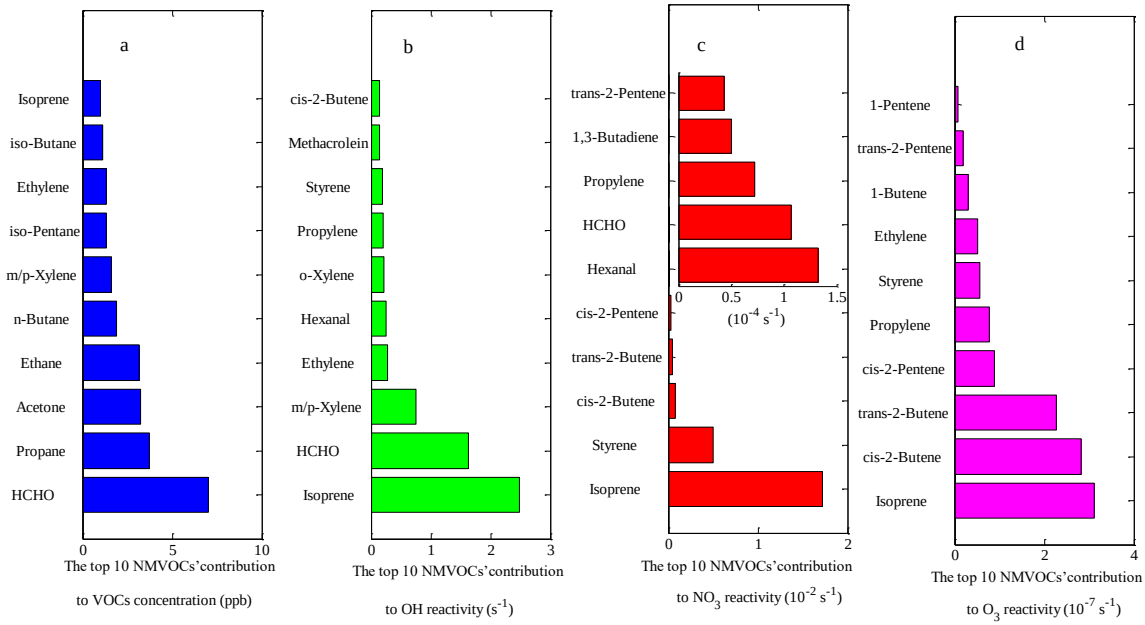

Figure 3. The top 10 NMVOCs' contribution to total NMVOCs concentration (a), OH reactivity (b), NO_3 reactivity (c) and O_3 reactivity (d)during the field campaign at Xianghe from 6 July to 6 August 2018.

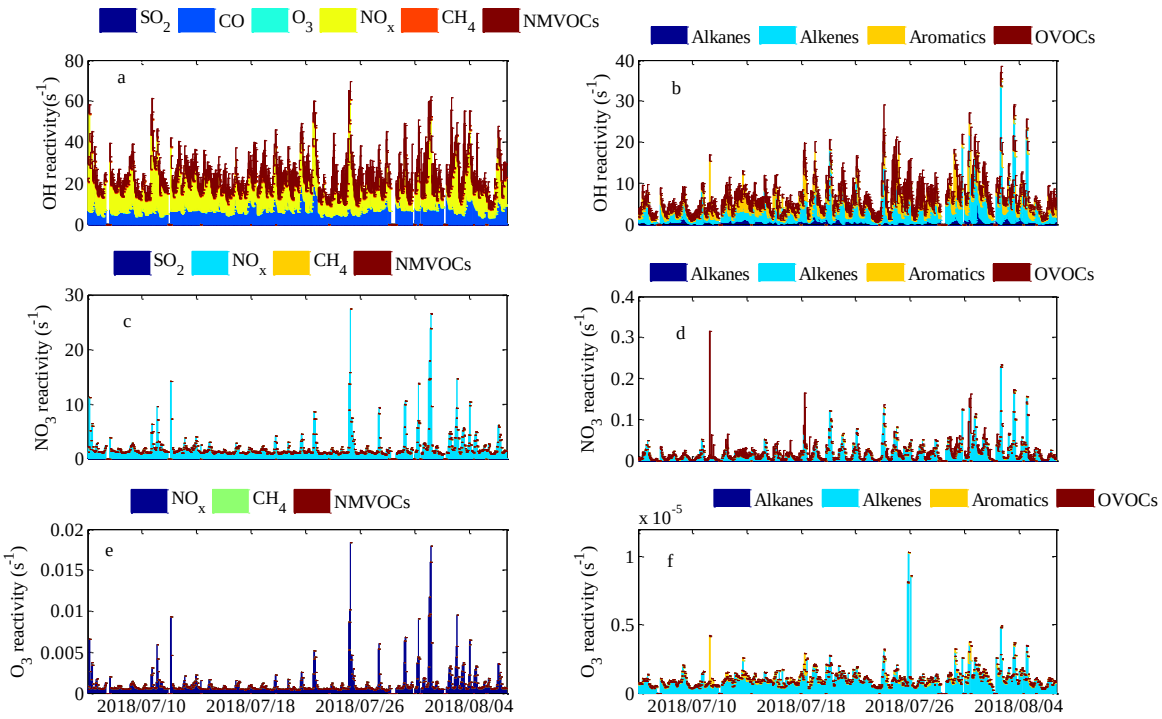

Figure 4. The time series of OH reactivity (a,b), NO_3 reactivity (c,d) and O_3 reactivity (e,f) during the field campaign at Xianghe from 6 July to 6 August 2018.

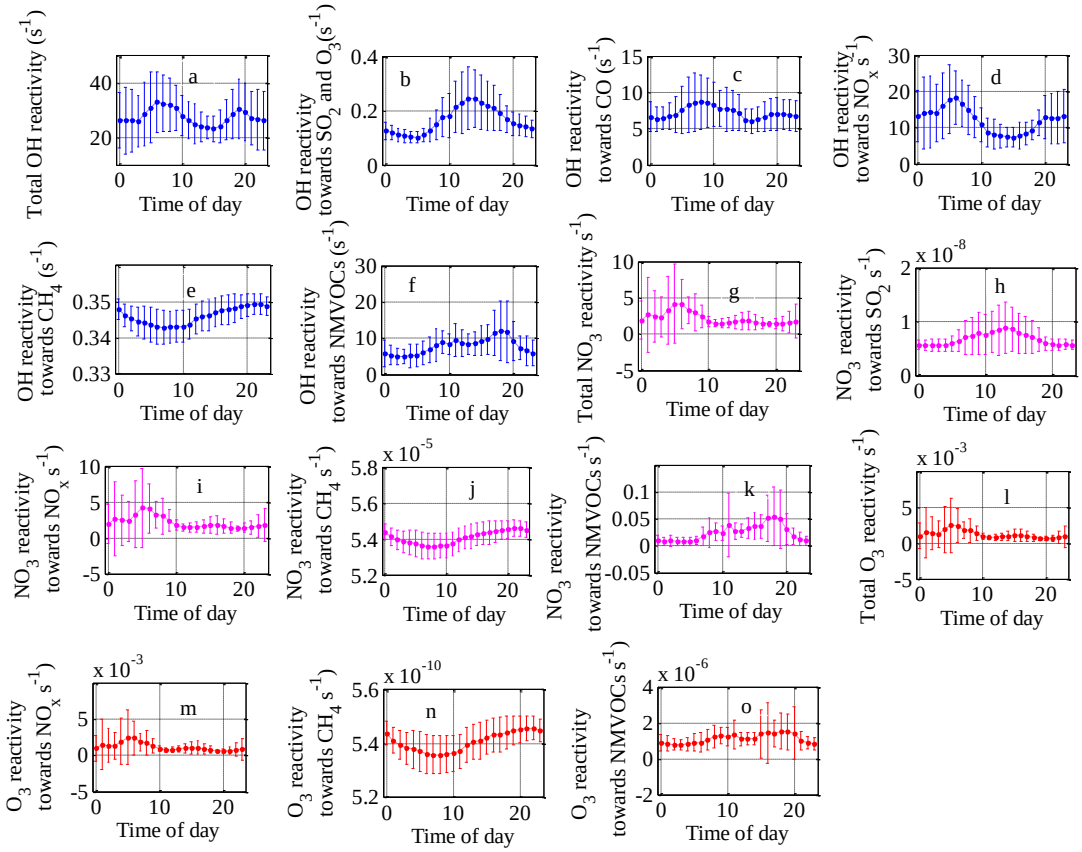

Figure 5. Mean diurnal variations of OH reactivity (a-f), NO_3 reactivity (g-k) and O_3 reactivity (l-o) of trace gases during the field campaign at Xianghe from 6 July to 6 August 2018.

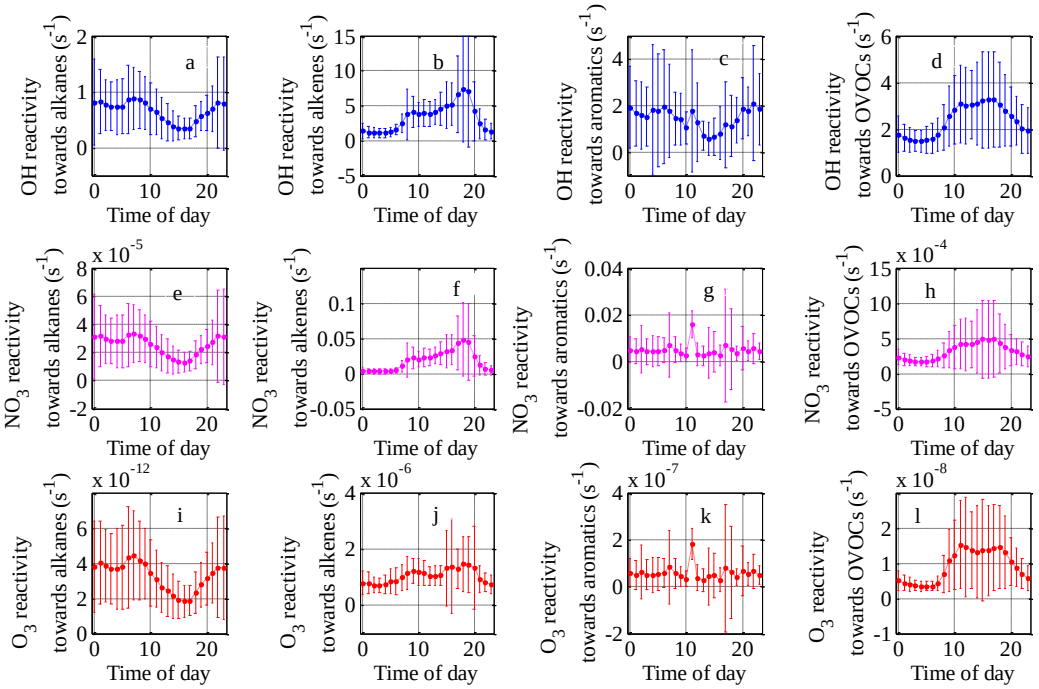

Figure 6. Mean diurnal variations of OH reactivity (a-d), NO_3 reactivity (e-h) and O_3 reactivity (i-l) of NMVOCs groups during the field campaign at Xianghe from 6 July to 6 August 2018.

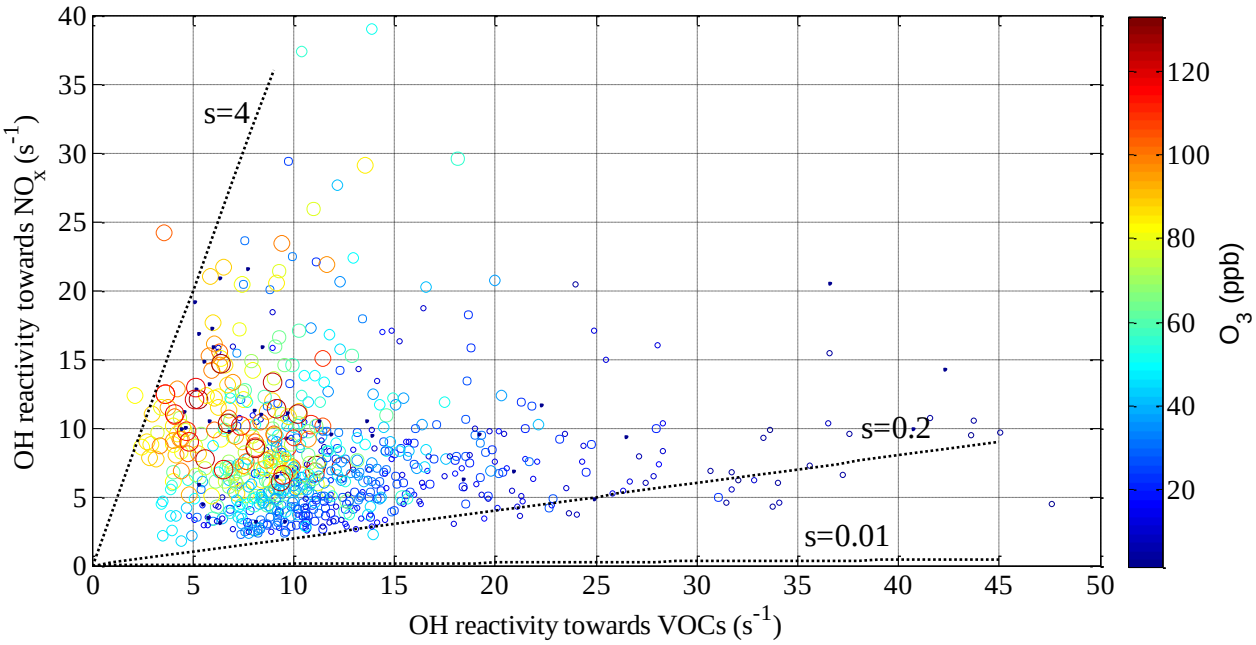

Figure 7. O_3 production regimes at Xianghe station. The dot lines are the borders of the three regimes of O_3 formation. "s" denotes the relative reactivity of OH towards NO_x and VOCs. For s > 0.2: VOC limitation, for s < 0.01: NO_x limitation of the O_3 formation.

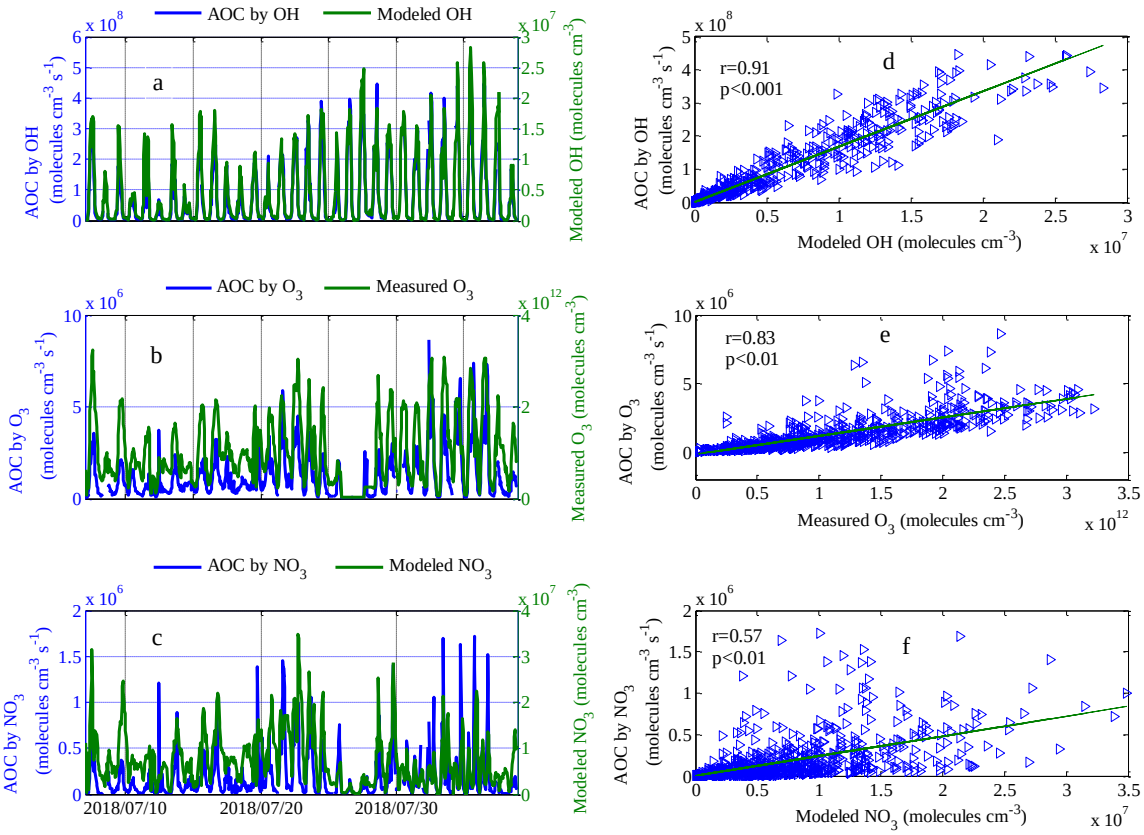

Figure 8. Comparisons of calculated AOC by modeled OH (a), measured O_3 (b) and modeled NO_3 (c), and corresponding oxidation concentrations. The left column shows the time series and the right column shows scatterplots of calculated AOC and corresponding oxidation concentrations. Note: r and p are the correlation coefficient and the significance level, respectively.

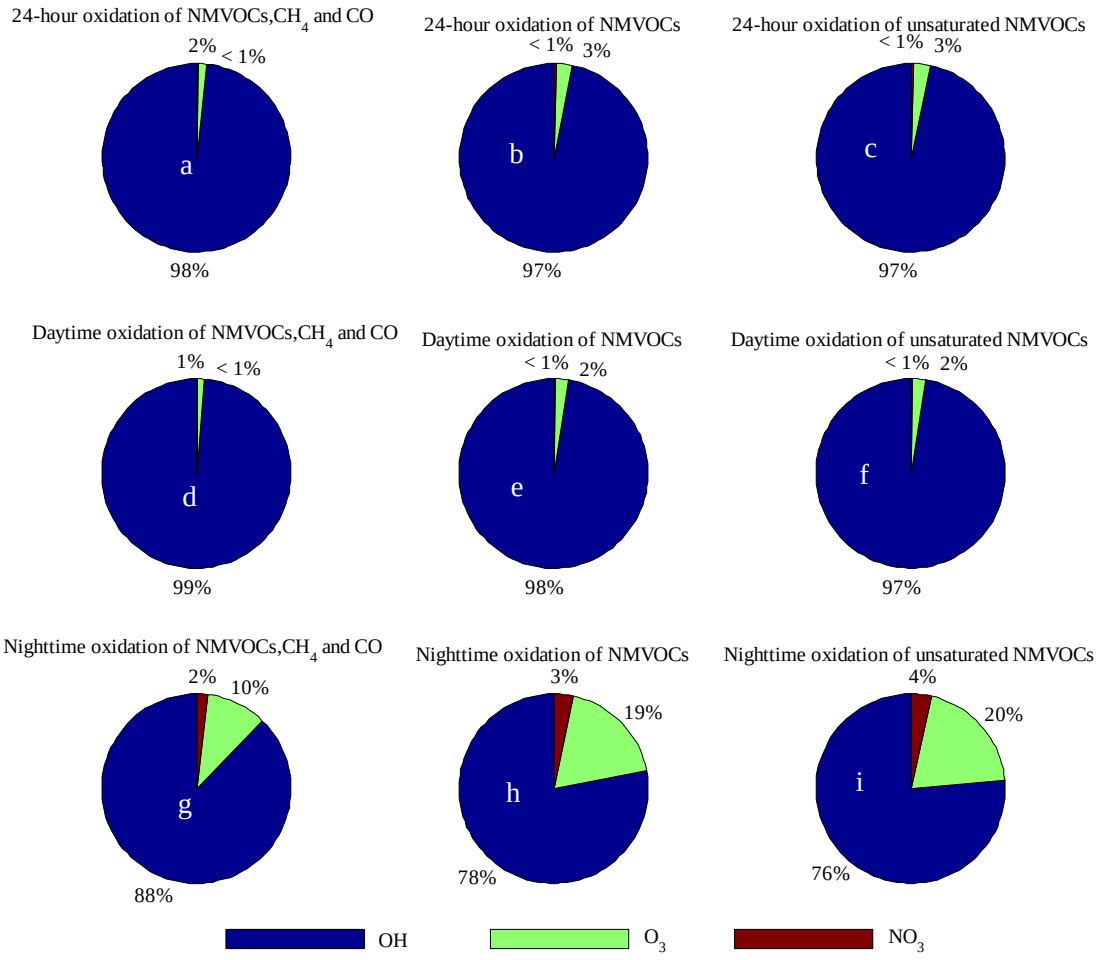

Figure 9. Comparison of the relative contributions of OH, NO_3 and O_3 to the 24-h, daytime and nighttime averaged loss rates. Data are calculated for the loss rates of (a, d and g) NMVOCs, CH_4 and CO, (b,e and h) NMVOCs only, and (c,f and i) unsaturated NMVOCs only.

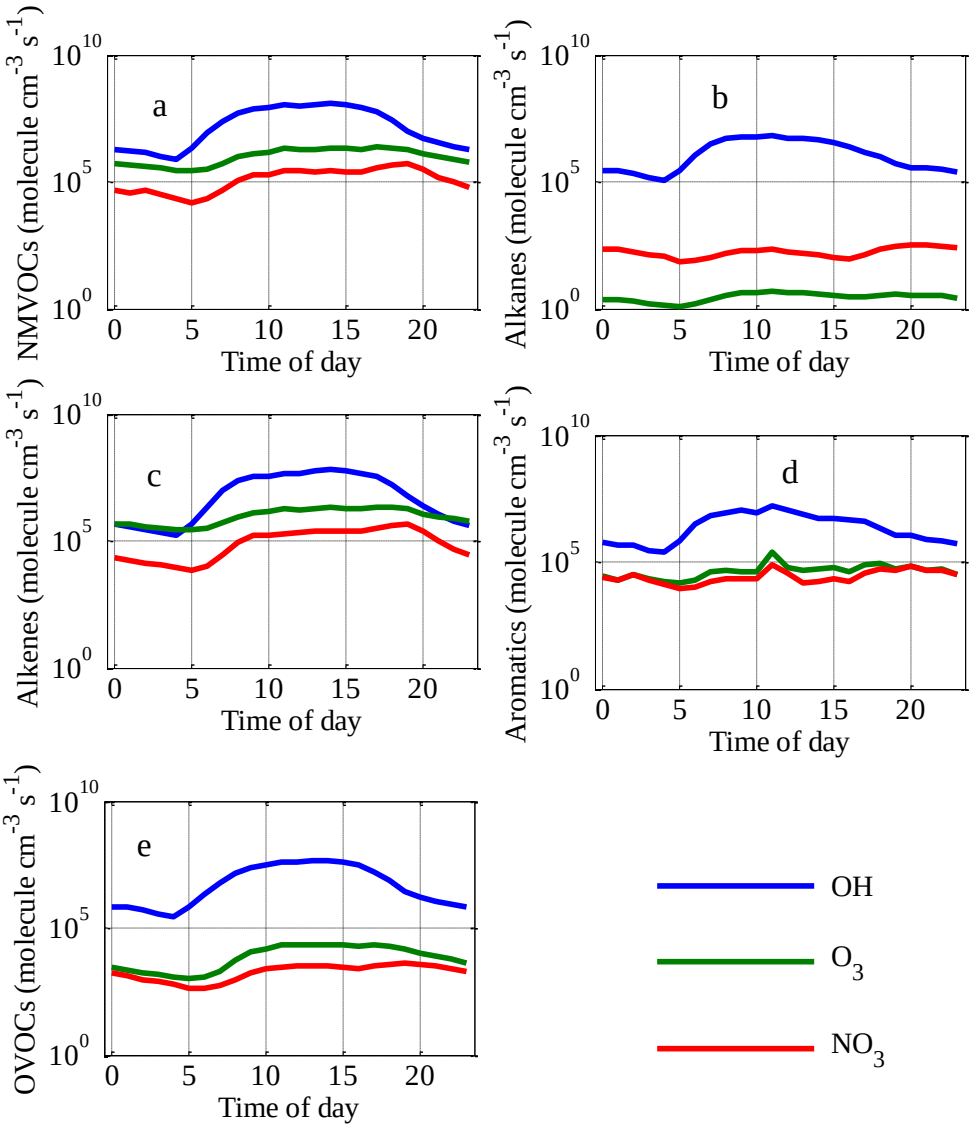

Figure 10 . Diurnal variations of NMVOCs loss rates due to the reactions with OH radical (blue lines), O_3 radical (green lines) and NO_3 (red lines).

Table captions

Table1. Comparison of speciated OH reactivity with former studies in China.

Species	This study	Beijing[a]	Shangdianzi[a]	Heshan[b]	Guangzhou[c]	Chongqing[c]	Beijing[d]	Shanghai[e]
CH_4	0.346							0.34
Ethane	0.019	0.01	0.01	0.023	0.24	0.59		
Propane	0.100	0.32	0.10	0.081				
iso-Butane	0.058	0.45	0.12	0.075				
n-Butane	0.111	0.09	0.08	0.104				
Cyclopentane	0.001	0.08	0.03	0.011				
iso-Pentane	0.119	1.18	0.25	0.168				
n-Pentane	0.067	0.60	0.16	0.136				
2,2-Dimethylbutane	0.002	0.08	0.08	0.003				
2,3-Dimethylbutane	0.017	0.23	0.11	0.013				
2-Methylpentane	0.016	0.56	0.10	0.077				
3-Methylpentane	0.018	0.44	0.10	0.047				
n-Hexane	0.020	0.60	0.08	0.055				
2,4-Dimethylpentane	0.001			0.069				
Methylcyclopentane	0.019	0.49	0.07	0.024				
2-Methylhexane	0.003	0.22	0.04	0.035				
2,3-Dimethylpentane	0.001		0.00	0.007				
Cyclohexane	0.048	0.26	0.05	0.015				
3-Methylhexane	0.004	0.28	0.05	0.039				
2,2,4-Trimethylpentane	0.002	0.04	0.01	0.036				
n-Heptane	0.006	0.24	0.04	0.033				
Methylcyclohexane	0.003	0.25	0.03	0.015				
2,3,4-Trimethylpentane	0.001	0.03	0.01	0.031				
2-Methylheptane	0.002	-	0.00	0.007				
3-Methylheptane	0.001	0.11	0.03	0.007				
n-Octane	0.004	0.38	0.11	0.014				
Nonane	0.004	0.19	0.03	0.010				
n-Decane	0.003			0.008				
n-Undecane	0.002			0.006				
Ethylene	0.273	0.35	0.18	0.617	0.29	0.73		
Propylene	0.202	4.86	1.00	0.464	0.40	0.52		
trans-2-Butene	0.067	1.98	0.31	0.063				
1-Butene	0.100	1.65	0.73	0.077				
cis-2-Butene	0.145	1.33	0.32	0.084				
1,3-Butadiene	0.034	-	-	-				
1-Pentene	0.023	0.50	0.22	1.136				
trans-2-Pentene	0.006	0.64	0.13	0.066	0.31	0.26		
cis-2-Pentene	0.034	1.20	0.29	0.080				
Isoprene	2.463	5.59	2.81	0.862	0.31	0.92		

1-Hexene	0.007	-	-	0.018				
HCHO	1.797			1.153				
Acrolein	0.027			0.009				
Propanal	0.067			0.139				
Acetone	0.013			0.010				
MTBE	0.009			-				
Methacrolein	0.146			0.072				
n-Butanal	0.024			0.059				
MethylVinylKetone	0.138			0.039				
Methylethylketone	0.014			0.020				
2-Pentanone	0.001			0.001				
Pentanal	0.042			0.028				
3-Pentanone	0.001			0.002				
Hexanal	0.247			0.055				
Benzene	0.017	0.34	0.13	0.030				
Toluene	0.092	2.22	0.39	0.518	0.73	0.15		
Ethylbenzene	0.085	0.88	0.18	0.188				
m/p-Xylene	0.749	3.05	0.43	0.754	0.74	0.31		
o-Xylene	0.216	0.93	0.12	0.194	0.35	0.10		
Styrene	0.193	0.34	014	0.900	0.26	0.16		
Isopropylbenzene	0.002	0.04	0.01	0.004				
n-Propylbenzene	0.002	0.25	0.16	0.004				
m-Ethyltoluene	0.016			0.026				
p-Ethyltoluene	0.013			0.027				
1,3,5-Trimethylbenzene	0.031	2.90	1.08	0.042				
o-Ethyltoluene	0.006			0.018				
1,2,4-Trimethylbenzene	0.028			0.080	0.16	0.17		
1,2,3-Trimethylbenzene	0.008			0.028				
CO	7.196	6.90	5.37				9.13	3.15
NO	2.139						0.58	0.78
NO_2	9.947						4.08	2.87
SO_2	0.088						0.33	
O_3	0.076							

[a] (Xu et al., 2011); [b] (Yang et al., 2017); [c] (Tan et al., 2019); [d] (Liu et al., 2009); [e] (Zhu et al., 2020).

Table 2. The top 10 NMVOCs species in terms of concentration (first column), OH reactivity (second column), NO_3 reactivity (third column) and O_3 reactivity (fourth column) and their corresponding contributions to concentration, OH, NO_3 and O_3 reactivity towards NMVOCs (%).

First column					**Second column**				
Species	**Concentration**	OH reactivity	NO_3 reactivity	O_3 reactivity	**Species**	**Concentration**	OH reactivity	NO_3 reactivity	O_3 reactivity
HCHO	**22.3**	30.3	1.5	0.2	HCHO	22.3	**30.3**	1.5	0.2
Propane	**11.8**	1.9	0.1	0.0	m/p-Xylene	5.1	**14.0**	0.1	0.0
Acetone	**10.2**	0.3	0.0	0.1	Ethylene	4.2	**5.0**	0.1	6.1
Ethane	**6.0**	0.4	0.0	0.0	Hexanal	1.1	**4.6**	1.9	0.0
n-Butane	**5.1**	2.1	0.0	0.1	o-Xylene	2.1	**4.0**	0.1	0.0
m/p-Xylene	**4.3**	14.0	0.1	0.1	Propylene	1.0	**3.7**	1.0	9.0
iso-Pentane	**4.2**	2.2	0.1	0.1	Styrene	0.4	**3.6**	70.2	6.6
Ethylene	**4.4**	5.0	0.1	6.1	Methacrolein	0.7	**2.7**	0.2	0.7
iso-Butane	**3.5**	1.1	0.0	0.0	cis-2-Butene	0.3	**2.7**	11.2	33.0
n-Pentane	**2.3**	1.3	0.0	0.0	MethylVinylKetone	0.9	**2.6**	0.1	0.0
Third column					**Forth column**				
Species	**Concentration**	OH reactivity	NO_3 reactivity	O_3 reactivity	**Species**	**Concentration**	OH reactivity	NO_3 reactivity	O_3 reactivity
Styrene	0.4	3.6	**70.2**	6.6	cis-2-Butene	0.3	2.7	11.2	**33.0**
cis-2-Butene	0.3	2.7	**11.2**	33.0	trans-2-Butene	0.2	1.3	6.6	**26.5**
trans-2-Butene	0.2	1.3	**6.6**	26.5	cis-2-Pentene	0.1	0.8	3.5	**10.3**
cis-2-Pentene	0.1	0.8	**3.5**	10.3	Propylene	1.0	3.7	1.0	**9.0**
Hexanal	1.1	4.6	**1.9**	0.0	Styrene	0.4	3.6	70.2	**6.6**
HCHO	22.3	30.3	**1.5**	0.2	Ethylene	4.2	5.0	0.1	**6.1**
Propylene	1.0	3.7	**1.0**	9.0	1-Butene	0.4	1.9	0.6	**3.6**
1,3-Butadiene	0.1	0.6	**0.7**	0.4	trans-2-Pentene	0.0	0.1	0.6	**2.2**
trans-2-Pentene	0.0	0.1	**0.6**	2.2	1-Pentene	0.1	0.4	0.2	**0.9**
1-Butene	0.4	1.9	**0.6**	3.6	Methacrolein	0.7	2.7	0.2	**0.7**